

Temple University

College of Engineering

Bioengineering

Design Document

Partial Gravity Bioreactor

Presented By: Team #13

Dmitry M Hackel

Irene Bui

Jake Fisher

Zenub Abouzid

Supervised By:

Dr. Yah-el Har-el & Dr. Peter Lelkes

1 2 – 0 8 – 2 0 2 5

Acknowledgment

We want to extend our most profound appreciation to the following individuals and organizations who have contributed to the completion of this project:

- Dr. Jonathan Gerstenhaber, for providing valuable information on previous prototypes, coding, debugging, and ideas that paved the way for the prototype, and for delivering his lab time and office hours for us to finalize our prototype.
- Dr. Michael Phelan, for allowing us to use his air-bubble-bioreactor
- Dr. James Furmato, for allowing us to use the laboratory during his lectures.
- PhD Candidate Jennifer Patten and PhD Student Shaylyn Westmoreland, for providing the materials in the lab and being present to supervise the laboratory validation test.
- Brian Amin and Matthew Short, a previous team who completed a similar topic, for giving us the time to explain their prototype in more depth.
- Ahmed Satour and Muhammed Hassan, for aiding in the program.
- The 2nd floor mechanical shop, lab coordinators, and students who kindly helped us with the issues faced during the build.
- Temple University, for providing access to their machines, labs, and space.

Additionally, we would like to express our gratitude to all those who have supported us in both visible and unseen ways. Without your contributions and presence, this project would not have been possible.

Thank you.

Abstract

The progress of human exploration to space, the Moon, and Mars is not considered safe because of the limited understanding of how partial gravity impacts human cells. This issue has not been fully addressed due to cost limitations and the lack of validation of partial gravity on Earth. This project focused on developing a validated prototype for a partial gravity bioreactor. By successfully simulating the mathematical model and conducting tests to validate the prototype, a better understanding of whether partial gravity is achieved and its limitations can be discussed.

Table of Contents

LIST OF ACRONYMS/ABBREVIATIONS.....	VI
LIST OF FIGURES.....	I
LIST OF TABLES	II
1. PROBLEM STATEMENT.....	1
1.1 OVERALL OBJECTIVE	1
1.2 BACKGROUND.....	2
1.3 NEEDS STATEMENT.....	6
1.4 IMPLICATIONS OF PROJECT SUCCESS	6
2. DESIGN CRITERIA	8
2.1 NON-NEGOTIABLE CRITERIA	8
2.2 NEGOTIABLE CRITERIA.....	10
3. SOLUTIONS	12
3.1 BIOREACTOR SOLUTIONS	12
SOLUTION R.A: STANDARD BIOREACTOR	12
SOLUTION R.B: BUBBLE CATCHER BIOREACTOR	13
3.2 PARTIAL GRAVITY SOLUTIONS.....	14
SOLUTION P.A: INCLINED PLANE (DUAL MOTORS).....	14
SOLUTION P.B: FOUR CENTRIFUGATIONS	16
SOLUTION P.C: INCLINED PLANE (SINGLE MOTOR).....	18
3.3 DECISION MATRIX	20
4. ENGINEERING DESIGN.....	22
4.1 DESIGN RATIONALE	22
4.2 CALCULATIONS	25
INCLINE PLANE	25
CENTRIPETAL ACCELERATION.....	27
ANGULAR VELOCITY	29
RPM	30
LINEAR VELOCITY	30
SEDIMENTATION VELOCITY	31
DYNAMIC PORTION	36
4.3 NUMERICAL SAMPLING.....	38
CORRELATION AND ANALYSIS.....	38
4.4 SIMULATION	39
MATHEMATICAL SIMULATION.....	39

5. COMPONENTS.....	41
5.1 MOTOR, DRIVER, AND MICROCONTROLLER.....	41
5.2 BASE MATERIAL	43
5.3 ROD	44
5.4 BIOREACTOR	44
6. PROTOTYPE.....	46
6.1 WIRING.....	46
6.2 OVERALL PROTOTYPE BASICS.....	47
7. TEST METHODS.....	50
8. RESULTS	51
RPM AND TILT VALIDATION TESTS	51
ALGINATE BEAD TEST	52
INDIRECT CONTACT TEST	53
9. COST	54
10. SUMMARY AND CONCLUSION	55
11. REFERENCES	57
12. SUPPLEMENTARY DATA.....	62
13. SUPPLEMENTARY DATA REFERENCES	64

List of Acronyms/Abbreviations

MOND	Modified Newtonian Dynamics
ACME	Advanced Combustion via Microgravity Experiments
NASA	The National Aeronautics and Space Administration
ISS	International Space Station
0G	Zero Gravity
μG	Microgravity
$\frac{1}{6}G$	Lunar Gravity
$\frac{3}{8}G$	Martian Gravity
1G	Earth Gravity
RWV	Rotating Wall Vessel
UNSDG	United Nations Sustainable Development Goals
SDG	Sustainable Development Goals
DGD	Degree of Gravity Dispersion
RGP	Reduced Gravity Paradigm
STLV	Slow-Turning Lateral Vessel
HARV	High Aspect Ratio Vessel
MAGICIAN	Mars Artificial Gravity Habitat with Centrifugation

List of Figures

FIGURE 1. EXPERIMENTAL DESIGN FOR SIMULATED PARTIAL GRAVITY APPARATUS FOR RATS	3
FIGURE 2. BASIC BIOREACTOR.....	4
FIGURE 3. 3D CLINOSTAT.....	5
FIGURE 4. PARTIAL GRAVITY BIOREACTOR.....	6
FIGURE 5. SCHEMATIC SIDE VIEW OF ROTATING WALL VESSEL BIOREACTOR	12
FIGURE 6. DESIGN OF BIOREACTOR	13
FIGURE 7. BUBBLE TRAPPING BIOREACTOR SKETCH	14
FIGURE 8. INCLINED PLANE BIOREACTOR WITH DUAL MOTORS	15
FIGURE 9. ROUGH SKETCH OF INCLINED PLANE WITH DUAL MOTORS	16
FIGURE 10. SCHEMATIC DIAGRAM OF CENTRIFUGATION TO SETTLE PARTICLES.....	17
FIGURE 11. ROUGH SKETCH OF THE CENTRIFUGATION SOLUTION.....	17
FIGURE 12. ROUGH SKETCH OF INCLINED PLANE WITH SINGLE MOTOR.....	19
FIGURE 13. STLV vs HARV.....	23
FIGURE 14. ORBIT TRAJECTORY OF THE CELL WITHIN A ROTATING BIOREACTOR	24
FIGURE 15. MAGAICIAN SCHEMATIC	24
FIGURE 16. FREE BODY DIAGRAM OF A BIOREACTOR ON AN INCLINED PLANE	25
FIGURE 17. FREE BODY DIAGRAM OF THE PARTICLE IN FLUID.....	32
FIGURE 18. RPM VS RADIUS	39
FIGURE 19: PARALLEL GRAVITY COMPONENT FOR EARTH AND MARS	40
FIGURE 20: HARV LAYERS	45
FIGURE 21: ELECTRICAL SCHEMATIC.....	47
FIGURE 22. PROTOTYPE DIMENSIONS (INCHES)	47
FIGURE 23. ISOMETRIC VIEW OF PROTOTYPE CAD.....	48
FIGURE 24: PROTOTYPE ANGLED VIEW	49
FIGURE 25. RPM AND TILT VALIDATION.....	52
FIGURE 26. ALGINATE BEAD PARTICLE MOTION.....	52
FIGURE 27. CELL VIABILITY PER MATERIAL	53

List of Tables

TABLE 1. NON-NEGOTIABLE NEEDS	10
TABLE 2. NEGOTIABLE NEEDS.....	11
TABLE 3. DESIGN MATRIX FOR RWV SOLUTIONS	21
TABLE 4. DESIGN MATRIX FOR PARTIAL GRAVITY SOLUTIONS.....	21
TABLE 5. NUMERICAL VALUES OF INITIAL RPM AND ANGLE VALUES.....	38
TABLE 6: MATERIAL COST	54
TABLE 7: PROTOTYPE CRITERIA	55

1. Problem Statement

1.1 Overall Objective

Since the 1960s, space exploration has yielded intriguing discoveries that continue to unfold. Yuri Gagarin became the first human in space in 1961, paving the way for thousands of astronauts and cosmonauts to follow him as the years passed [1]. Various theories have been proposed based on space, including the Croatian Barrel Theory, which explains how the solar system, stars, and other celestial bodies formed [2], [3]. In 2002, research refuted the theory that gravity alone governs the universe, as it could not explain specific astronomical observations [4]. Sanders and McGaugh modified Newtonian gravity as an alternative to cosmic dark matter, known as Modified Newtonian Dynamics (MOND), correlating the Newtonian acceleration with the observed acceleration at any radius in a galaxy [5], [6].

Exploring space not only reveals discoveries beyond our planet but also uncovers truths that shape and govern our lives. Advanced Combustion via Microgravity Experiments (ACME) investigates fuel efficiency and pollutant production in combustion under microgravity conditions on Earth [7]. One of their investigations, Flame Design, studied the quantity of soot produced under different flame conditions [7]. Such a discovery could lead to more efficient combustion, reducing pollution on Earth [7]. In the ongoing Moon exploration, researchers found that the Moon's gravity affects Earth's tides, plant growth, animal behavior, and agricultural practices [8]. Moreover, models have shown that the Earth-Moon coupled magnetospheres provide a buffer against the solar wind, allowing for a reduction in Earth's atmospheric loss to space [9]. The National Aeronautics and Space Administration (NASA) has been exploring Mars for over sixty years to decide whether it is or was a habitable world [10]. Since Mars is the most similar planet to Earth, understanding its surface and evolution is crucial for preparing for future human exploration [11]. With evidence suggesting that Mars was once full of water, warmer, and had a thicker atmosphere, it is highly likely that Mars could be a habitable environment [11].

Traveling beyond Earth's atmosphere to investigate potential extraterrestrial life entails considerable risks and substantial financial investment. Given that human physiology is heavily dependent on gravity, significant fluctuations in the gravitational force may lead to serious health issues [12]. Gravity, as a vector quantity, influences all objects by determining their weight relative to their mass [13]. Biological organisms respond to environmental stimuli—including gravity—by developing unique morphological traits, physiological characteristics, behaviors, and habitat preferences [13]. The sensitivity of organisms to changes in gravity increases with their size and mass, with single cells enduring exposures up to 10^5 G and humans tolerating gravitational forces of 4-5G [13]. At the cellular level, cells comprise organelles, each with mass and thus subject to gravitational forces [14]. Variations in gravitational vectors could disrupt cellular homeostasis, affecting structural integrity, composition, and orientation, such as the cytoskeleton, which maintains cellular shape [14]. Additionally, numerous studies have documented genes that are sensitive to gravity alterations, including alterations in cytoskeletal gene expression pathways and gene inhibition following microgravity exposure [15], [16]. In the absence of gravity, cellular growth pathways shift, and metabolic processes adapt due to changes in reactive oxygen species levels [17], [18].

Furthermore, cellular adaptation to gravity is crucial for tissue adaptation, as bones contain osteocytes that sense and respond to varying gravitational loads [13].

Such cellular changes impact the entire human system. Astronauts exposed to microgravity undergo physiological deconditioning in systems sensitive to mechanical loading, including the cardiovascular, pulmonary, and musculoskeletal systems [19]. To mitigate these effects, International Space Station (ISS) crew members engage in rigorous exercise; however, despite extensive physical activity, astronauts still return from their six-month ISS missions exhibiting decreased calf muscle volume and strength, loss of bone mineral density, and reduced peak oxygen uptake [20], [21], [22], [23].

Given that, it is highly unethical to send people into space without understanding the effects of gravitational changes on the body. This paper discusses a validated prototype of a device that cultures cells under partial gravity and microgravity, enabling the correlation of specific cell behaviors with gravitational conditions.

1.2 Background

Understanding the effects of partial gravity on humans is less well studied due to the high costs of conducting tests in partial or microgravity environments. Between 1960 and 1973, the research experience and studies gained during the Apollo missions—focused on lunar exploration—provided valuable insights into the diverse effects of partial gravity on the human musculoskeletal, cardiovascular, and respiratory systems, employing either microgravity or Earth’s gravity as controls [23], [24]. However, the Apollo missions cost approximately \$25.4 billion in 1969, equivalent to roughly \$217 billion in 2024 [25]. Following these missions, despite the lack of subsequent lunar landings, the failures in early missions facilitated advancements in spacecraft design, including the incorporation of additional protective layers and the development of new, safer materials, as well as the integration of computer systems for troubleshooting purposes [26]. In 2019, the health impacts of a year-long space mission were examined at both the molecular and psychological levels by comparing the DNA sequences of twin brothers, Mark and Scott Kelly, with Mark Kelly remaining on Earth serving as the control, and Scott Kelly participating in spaceflight [27], [28]. The study revealed that extensive changes in multisystem and gene expression occur during spaceflight [28]. Astronauts may face risks including mitochondrial dysfunction, immunological stress, vascular modifications, fluid shifts, and cognitive performance decline, as well as alterations in telomere length, gene regulation, and genome integrity [28].

Given the costs and decommissioning of the ISS, researchers endeavored to replicate partial gravity conditions on Earth, such as using a pulley-spring system to simulate partial gravity for rodents (see [Figure 1](#)) [23], [29]. However, a limitation of the apparatus was that only the tail was suspended rather than the entire body, resulting in a weight shift within the rodent’s body and thus failing to provide a truly accurate simulation [29].

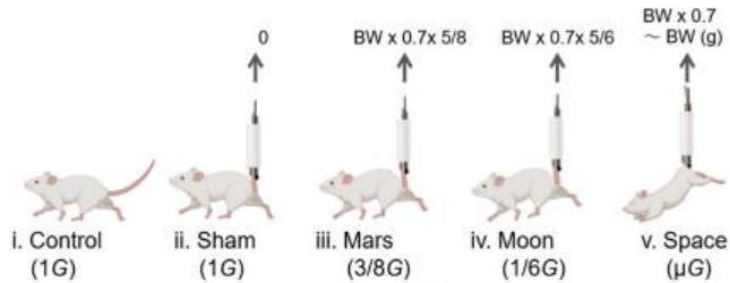


Figure 1. Experimental Design for Simulated Partial Gravity Apparatus for Rats

The figure shows the groups of experimental rats with (i) the Control group ($1G$); (ii) the sham group with SA ($1G$); (iii) the Mars group ($\frac{3}{8}G$); (iv) the Moon group ($\frac{1}{6}G$); and (v) the interplanetary space (μG) group [29].

The effects of gravity on an object may manifest as either displacement or deformation [30]. Microgravity creates distinctive environments conducive to cell growth, whereas partial gravity (such as on the Moon and Mars) may yield markedly different effects [31]. To comprehensively understand the concepts related to partial gravity apparatuses, it is imperative to distinguish between zero gravity, gravity, microgravity, and partial gravity. Gravity is an abstract phenomenon that can be quantified; however, its fundamental cause remains unknown [32]. The gravitational constant is not a force or acceleration but is employed as a scaling factor in Newton's Law of Gravitation, as demonstrated in [Equation 1](#)[32], [33].

$$F = \frac{Gm_1m_2}{r^2} \quad (1)$$

Equation 1. Gravitational Force Equation

Where:

F = gravitational force

m_1 = mass 1

m_2 = angle between the inclined plane and the base

r = distance between masses

G = universal constant ($6.67384 * 10^{-11} \frac{\text{m}^3}{\text{s}^2 \text{kg}}$)

Zero gravity ($0G$) describes a condition where there is an absence of gravitational force exerted on an object, which occurs either due to its infinite distance from any other gravitational body or when the net sum of all forces acting upon it equals zero [34]. Microgravity (μG) pertains to a state in which the net gravitational force exerted on an object is minimal, typically within the range of 10^{-4} to $10^{-6}G$ [35]. Although the object remains under the influence of gravitational forces, it continues to undergo free fall [35]. This perpetual free fall occurs when an object falls at a constant velocity without contacting a surface [35]. As a result, the difference between the initial and final velocities manifests as a constant acceleration (g) [35]. Partial gravity refers to a gravitational force that is diminished but not absent compared to Earth's gravitational acceleration, such as on the Moon, where gravity is approximately $\frac{1}{6}G$, on Mars $\frac{3}{8}G$, and on

Earth 1G [27]. On Earth, partial-gravity simulation can be achieved using techniques such as centrifugation, parabolic flight, or modified rotation devices that generate accelerations below 1 g [36].

To investigate gravitational effects, cell culturing is regarded as the most efficacious method, with bioreactors serving as the optimal apparatus, given their ability to supply controlled nutrients and biomimetic stimuli for cellular growth [37]. A bioreactor is defined as a vessel in which a chemical process involving organisms or biochemically active substances derived from such organisms is conducted, or a system designed for cell cultivation, first developed in 1964 (refer to [Figure 2](#)).

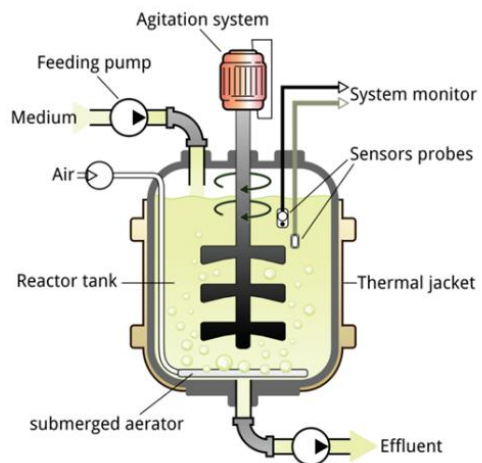


Figure 2. Basic Bioreactor

The figure shows the basic components of a bioreactor. It includes a feeding pump, air, medium, an agitation system, a reactor tank, and other elements to ensure an automated culturing system.

Previous bioreactors were designed as ground-based systems to mimic aspects of weightlessness or reduced gravity experienced by biological organisms in space. Recognizing this potential, in the mid-1980s, NASA researchers at the Johnson Space Center needed to develop a method to study the effects of microgravity on human tissues, as the shuttle fleet was grounded following the Challenger disaster [38]. They invented a rotating bioreactor to address the challenge of treating injured astronauts in space and to simulate weightlessness on Earth [38]. In μG , the bioreactor enables cells to grow in three-dimensional tissue structures that closely resemble natural development, facilitating advances in medicine both on Earth and in space [38]. In 2002, Houston-based Regenetech Inc. licensed NASA bioreactor technology and patents that can expand adult stem cells (from blood to bone marrow) by 50-200 times in less than a week, providing safer, faster, and more affordable cell sources for therapies [38].

Partial gravity bioreactors, although not extensively studied, have been previously examined. Research dating back to the 1900s has investigated the effects of clinostats, or rotating wall vessels, on biological samples [39]. Clinostats were invented by Julius Sachs, who rotated growing plants around their growth axis [39]. These devices exist in one-dimensional (1-D) or two-dimensional (2-D) forms, depending on the dimensions of the rotated axial line or the entire experimental area [40]. Subsequently, enhancements to the clinostat with two axes led to the development of three-dimensional (3-D) clinostats, known as the Random Positioning Machine (RPM) (refer to [Figure 3](#)) [40], [41].

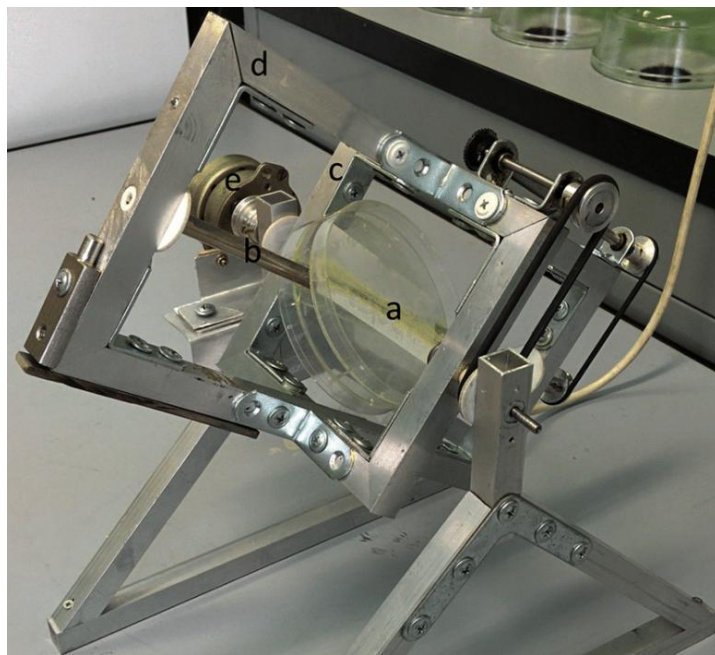


Figure 3. 3D Clinostat

The figure depicts a three-dimensional clinostat employed to investigate the effects of microgravity on seed germination: (a) insert for Petri dishes; (b) rotating shaft; (c) inner frame; (d) outer rotating frame; (e) motor [41].

Numerous early-stage partial-gravity bioreactors have been investigated using plant species capable of continuous growth under Earth's gravity [42]. Initial implementations included clinostats, which maintain a constant rotation of a sample to average the gravitational vector to near zero, effectively [39]. This partial gravity bioreactor does not fully replicate "true" microgravity, as cells continue to experience mechanical stimulation and gradients that differ from those in actual microgravity conditions [39]. Subsequently, rotating wall vessel (RWV) bioreactors were introduced as a specialized variant of clinostats [39]. RWVs are fluid-filled cylinders containing cells, designed to create a low-shear, controlled environment conducive to cellular differentiation in three-dimensional space [43]. By rotating at a terminal velocity, RWVs facilitate the proper delivery of nutrients to the tissue culture, thereby promoting healthy tissue and cell growth [45]. In 2018, a previous senior design team utilized the stability of RWVs for cell culturing while incorporating the partial gravity factor using an inclined plane to partially cancel the gravitational vector, allowing cells to experience a form of partial gravity (refer to Figure 4).

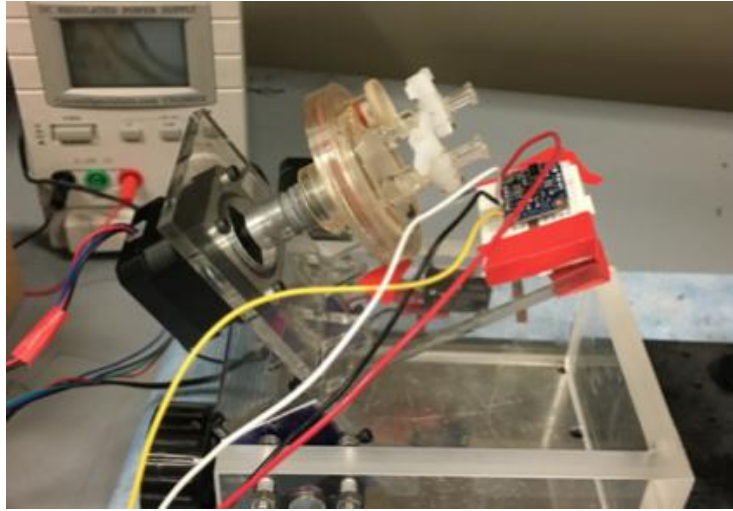


Figure 4. Partial Gravity Bioreactor

The figure depicts the prototype of a partial gravity bioreactor, designed by an earlier senior design team. It comprises an RWV affixed to an inclined plane that simulates partial gravity.

1.3 Needs Statement

There is a need to build a validated partial gravity cell-culturing prototype that would enable us to study the relationship between cell properties and different gravitational environments, thereby allowing us to correlate gravitational differences with cell properties.

1.4 Implications of Project Success

If the prototype succeeds, both terrestrial and extraterrestrial life would benefit significantly. Understanding the effects of varying gravitational conditions on cellular behavior would enable more precise conclusions about human space exploration. Such findings would underpin the development of solutions to safeguard human safety beyond Earth. Facilitating human travel to outer space, including destinations such as Mars and the Moon, enhances our understanding of extraterrestrial regions and addresses fundamental questions about alien life. Additionally, this research has the potential to identify new planets or locations in space where humans might establish a new life.

The success of the prototype closely correlates with several United Nations Sustainable Development Goals (UNSDGs) [44]. SDG 3: Good Health and Well-being is supported, as the device facilitates controlled studies on how partial gravity influences cellular development, physiology, and long-term health in space [45]. By understanding these effects, the prototype can inform the design of countermeasures, treatments, and potentially therapeutic approaches for conditions such as bone loss and muscle atrophy, which are of critical concern for astronauts [28]. Accordingly, the prototype would help ensure healthy lives for humans [45]. Furthermore, SDG 9: Industry, Innovation, and Infrastructure is pertinent, as the development of the prototype constitutes an innovative research platform that represents the convergence of biotechnology and space technology [46]. Additionally, the prototype advances SDG 12: Responsible

Consumption and Production by implementing a closed-loop biological system, an approach essential for sustainable space habitats and beneficial for the efficient utilization of resources on Earth [47]. The use of a bioreactor enhances system control during cell cultivation, enabling accurate, real-time monitoring, early problem detection, reproducibility, and cost efficiency [48]. In this context, SDG 13: Climate Action is addressed by demonstrating how biological systems adapt to extreme and changing environments, thereby informing strategies for Earth's ecosystems [49].

2. Design Criteria

To guarantee the feasibility of the prototype, the design criteria are classified as either non-negotiable (mandatory) (refer to [Table 1](#)) or negotiable (desirable) (refer to [Table 2](#)). However, owing to the complexity of the project, these criteria are divided into two primary domains: partial gravity and the prototype.

2.1 Non-Negotiable Criteria

Three criteria must be satisfied to deem the partial gravity component in the project successful: gravitational type, uniform trajectory, and mathematical simulation.

Gravitational Type: With NASA deorbiting the ISS, the ability to conduct experiments in the unique microgravity laboratories would be impossible. Therefore, gravitational experiments conducted on Earth should encompass the primary missions previously planned. According to NASA, traveling to the lunar surface and around the Moon would facilitate scientific discoveries that prepare humans for subsequent exploration, including Mars [50]. As the Moon and Earth represent the two most significant gravitational environments, lunar gravity ($\frac{1}{6}G$) and Martian gravity ($\frac{3}{8}G$) warrant careful consideration [51]. To obtain more accurate data, Earth's gravity (1G) and microgravity (μG) should also be included to ensure that the same cells are subjected to all gravity levels and to serve as references for previous experiments [51].

Uniform Trajectory: To cultivate cells effectively, the partial gravity method should not present any issues for cell culture practices. Given cells' high sensitivity to their environment, the technique used to simulate partial gravity must prevent excessive vibrations or inconsistent cell motion [52]. To accomplish this, the procedure for attaining different gravitational levels should function smoothly, enabling cells to undergo free fall while simultaneously minimizing shear stress on the cells and maintaining these conditions continuously.

Mathematical Simulation: The partial gravity effect on cells has not yet been observed or tested. However, visualizing gravity is not applicable, since gravity is a theory [53]. Utilizing mathematics, fluid mechanics, and particle mechanics, a mathematical model should be developed for partial gravity.

Four criteria should be met to consider the prototype successful: overall device size, electrical safety, emergency safety, and material.

Overall Device Size: Since the prototype's placement may be limited to the incubator, its overall dimensions are also constrained. The Nuaire NU-5810E incubator is considered the most suitable and effective location based on previous designs because it operates at 37°C with 98% humidity [54]. The maximum size of the prototype is limited by the incubator's internal capacity, which measures 23 × 17 × 14 in.

Electrical Safety: For electrical safety, the standards established by the International Electrotechnical Commission (IEC), specifically IEC 60204-1, which outlines the general requirements for electrical equipment of machines (related to the safety of machinery), will be followed [55]. According to 'Safety of Machinery - Electrical Equipment of Machines - Part 1: General Requirements', a protective bonding circuit is required, ensuring all exposed metallic parts of the machinery are bonded and connected to a reliable ground [55]. This includes electrical enclosures and wiring, which should be organized neatly, clearly labeled, and protected, with cables rated appropriately for the voltage and current they carry [55]. Complying with EN 61010-2-030, Measuring Circuits and Test Equipment Safety Test, ensures the standard is met [56]. Since this is a prototype, comprehensive documentation—including electrical schematics, wiring diagrams, component lists, and user manuals—is essential.

Emergency Safety: As the prototype involves mechanical motion, there exists a potential for malfunctions. Consequently, ensuring the machinery's safety is imperative. The International Standard ISO 13850, titled "Emergency Stop Function, the Design Principles for the Emergency Stop Function on Machinery", stipulates that an emergency stop is mandated when the machine presents a risk, and its implementation would mitigate this risk, as applicable to the prototype [57]. To comply with this standard, the emergency stop function should be activated by a human-initiated signal that remains engaged until it is manually reset [57]. Additionally, no start command should be effective during the operations halted by the emergency stop initiation, which must likewise be reset through human intervention [57].

Material: Given the potential placement of the prototype within an incubator, the selected materials must withstand room temperature, 37°C, and 98% humidity [54]. Furthermore, the prototype is expected to remain stable for safety concerns.

Table 1. Non-Negotiable Needs

#	Priority	Requirement	Metric	Target Values/ Range or Pass/Fail	Justification
1	Non-negotiable	Gravitational Type	Partial Gravity and Controls	Range: μG to $1G$ Lunar gravity ($\frac{1}{6}G$) Martian gravity ($\frac{3}{8}G$) Earth's gravity (1G) Microgravity (μG)	NASA's Goals [50]
2	Non-negotiable	Uniform Trajectory	Partial Gravity Accuracy	Pass/ Fail Using Model and Visuals	Inaccuracy of data due to cell sensitivity [52]
3	Non-negotiable	Mathematical Simulation	Mathematical Model	Pass/ Fail	Accuracy and Validation
4	Non-negotiable	Overall Device Size	Dimensions	$23 \times 17 \times 14 \text{ in}$	Nuaire NU-5810E Incubator Restricted Area [54]
5	Non-negotiable	Electrical Safety	Safety	Pass/ Fail of EN61010-2-030	IEC 60204-1 [55, p. 60]
6	Non-negotiable	Emergency Safety	Safety	Pass/ Fail of ISO 13850	ISO 13850 [57]
7	Non-negotiable	Material	Strength, Durability, and Sterility	Pass/ Fail to withstand room temperature and 37°C , along with 98% humidity [54]	Safety

The table outlines the seven non-negotiable criteria essential for validating the prototype. Regarding partial gravity, the requirements encompass gravitational type, uniform trajectory, and mathematical simulation. Regarding the prototype, the requirements related to the base and partial gravity—such as overall device size, electrical safety, emergency safety, and material—are considered fundamental. Additionally, the metric, target range, and justification for each criterion are systematically provided.

2.2 Negotiable Criteria

Regarding the negotiable criteria, three factors could enhance the prototype if implemented. First, ensuring that the materials in contact with the cells are non-toxic would ensure that the prototype is suitable for cell culturing, with a cell viability exceeding 80%, in accordance with ASTM F2739-19 [58]. Additionally, integrating an automated imaging system for cellular analysis would enable users to comprehensively evaluate cell culture and gain deeper insights into cellular interactions across different temporal stages. Finally, advancing mathematical models into computational simulations would facilitate a more detailed understanding of the fluid dynamics affecting cells.

Table 2. Negotiable Needs

Priority	Requirement	Metric	Target Values/ Range or Pass/Fail	Justification
Negotiable	Cell Viability	Proper Cell Culture	>80%	ASTM F2739-19 [58]
Negotiable	Automated Imaging System	Data Tracking	> 30 FPS	To record the cell's activity during culturing
Negotiable	Computational Models	Modeling Accuracy	Pass/ Fail	To have a more sophisticated model for partial gravity

The table outlines the three negotiable criteria for enhancing the prototype. These criteria encompass cell viability, an automated imaging system, and the development of computational models. The table supplies the metric, target range, and justification for each criterion.

3. Solutions

The project focuses on validating partial gravity by ensuring the tested specimen experiences the intended gravitational force. Cell culturing methodologies will not be addressed. To eliminate any effects attributable to cell culture, the same culture component will be used across all proposed solutions.

3.1 Bioreactor Solutions

Bioreactors are the predominant method used in cell cultivation due to their ability to sustain biologically active environments and regulate parameters such as pH, temperature, oxygen tension, media perfusion rate, as well as their capacity to apply external stimuli [59]. Various types of bioreactors exist, including wave motion, stirred-tank, and rotating-wall vessels (refer to [Supplementary Table S1](#)) [37]. Since cells are susceptible to mechanical stresses such as shear forces and microfluidic flow, which may result in cellular structural failure and reduced viability, the selection of a bioreactor should be based on its ability to exert minimal shear stress on the cells [60]. Cells cultured in microgravity and ground-based microgravity analogs are presented with a low-shear stress environment suitable for cell cultivation [61]. RWVs are effective for small volumes (< 10 L) and can simulate microgravity with low turbulence and minimal impact [37].

Given the same bioreactor used for cell cultivation, two potential RWV configurations are examined. The solutions are based solely on the RWV's bubble issue.

Solution R.A: Standard Bioreactor

RWVs have been observed extensively to provide continuous particle sedimentation through a culture medium [62]. The rotation provided by the RWV is special since it induces minimal cellular shear and turbulence [62]. [Figure 5](#) shows the side view of a rotating wall vessel [63].

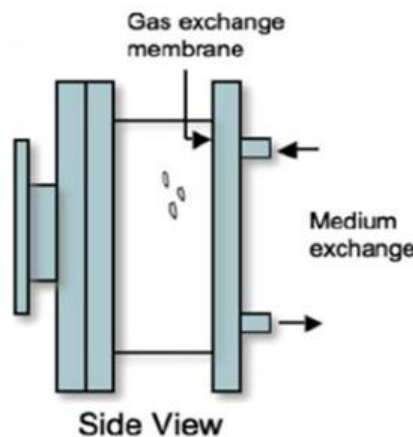


Figure 5. Schematic Side View of Rotating Wall Vessel Bioreactor

The rotation facilitates the complete immersion of the particle seeded in the medium. Consequently, using the standard RWV advances knowledge in cell culture. RWV systems have demonstrated success in cultivating prostate organoids, liver tissue, colon carcinoma, cartilage, and many other cell types [63].

Solution R.B: Bubble Catcher Bioreactor

One complication associated with RWVs is the formation of bubbles during operation [64]. The formation of bubbles interferes with the RWV environment, which includes zero headspace, low shear, and simulated microgravity [64]. Laminar flow must be established so that the liquid in the bioreactor behaves as a rotating body. A novel bubble-capture HARV design would reduce and potentially eliminate the common issues of bubble formation while also reducing operational media volume without compromising the radius.

The bioreactor is designed with a hollow, microporous plastic tube and an exit channel to capture bubbles (see [Figure 6](#)). The small, hollow tube, made of sponge-like plastic with tiny pores, has a plug placed partway down its length. When media is pushed down the tube, an exchange of old and new media occurs, providing nutrients to the circulating cells. This unique design enables direct filling of the main bioreactor chamber, with the output routed through a channel that captures bubbles and facilitates the exchange of used media (as shown in [Figure 7](#)) [64].

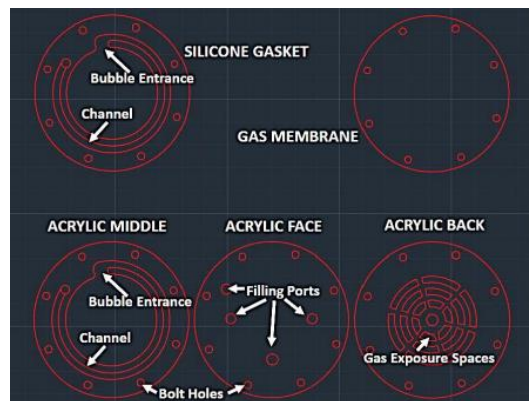


Figure 6. Design of Bioreactor

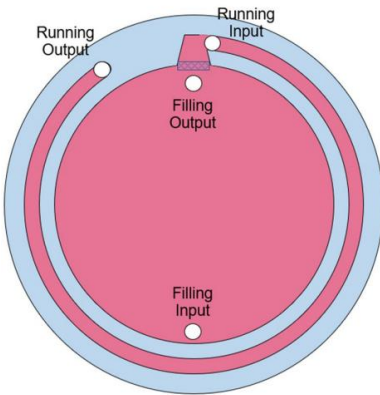


Figure 7. Bubble Trapping Bioreactor Sketch

Although this bioreactor design is more optimal, it can be successful only if the bioreactor is built and proven not to sustain any significant issues during construction within the short time available for this project. Furthermore, bubbles or flow disruptions do not simply represent mechanical inefficiencies; they directly affect cells' ability to remain in suspension, receive nutrients, and obtain oxygen. The presence of bubbles can also increase the shear forces affecting the cells.

3.2 Partial Gravity Solutions

Regarding partial gravity, three potential solutions are examined.

Solution P.A: Inclined Plane (Dual Motors)

The proposed solution entails enhancing an existing design by developing a partial gravity prototype using an RWV on an inclined plane, equipped with a dual-motor system (refer to [Figure 8](#)). The use of the inclined plane was previously studied and found to be a successful simulation of lunar gravity [65]. The design consists of three components: a foundational structure, a component that securely holds the bioreactor and the motor that generates rotational force, and a final system that adjusts the angle of the motor and bioreactor to simulate partial gravity.

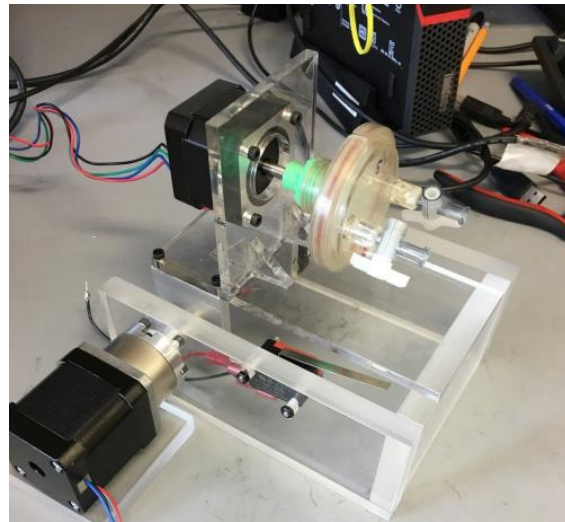


Figure 8. Inclined Plane Bioreactor with Dual Motors

The figure depicts the inclined-plane bioreactor designed by the previous senior design team. Utilizing two motors and an inclined plane, the previous team simulated partial gravity.

The base will be constructed as a rectangular structure capable of supporting the bioreactor assembly with stability and durability. The main section of the RWV will include a motor attached to the bioreactor to enable rotation, and this assembly will be mounted to the system that adjusts the bioreactor's angle. Next, a camera will be mounted on the same part of the device to accurately simulate the bioreactor's angle and monitor the cells during rotation within the RWV. For the final part, a secondary motor capable of adjusting to various angles will be used and attached to the bioreactor system. The secondary motor should be able to set angle variations at least at four different positions to mimic the following gravitational conditions: $1G$, $\frac{3}{8}G$, $\frac{1}{6}G$, and μG . The rough sketch of the proposed solution is seen in [Figure 9](#).

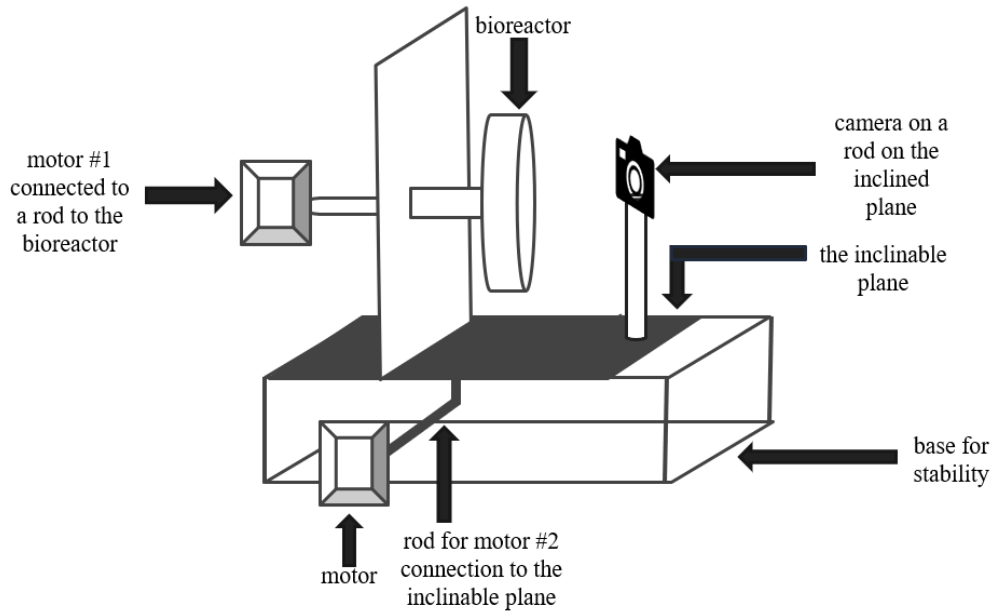


Figure 9. Rough Sketch of Inclined Plane with Dual Motors

The figure illustrates the preliminary sketch of the inclined plane setup with dual motors. The bioreactor is affixed to one motor, while the inclined plane is connected to another motor. The camera is positioned parallel to the bioreactor to ensure the entire bioreactor is captured in view.

These improvements to the current designs enhance the ability to validate the actual generation of partial gravities. The addition of a camera will enable real-time, accurate observation of cell reactions. Furthermore, this design provides a means for validation through modeling and mathematical analysis to confirm that this configuration produces the desired partial gravity effect for RWV.

Solution P.B: Four Centrifugations

The proposed solution concentrates on the centrifugation concept to emulate partial gravity on biological cells. The rationale for employing centrifugation is that centrifugal force generates an apparent gravity during rotational motion [66]. In fact, a proposed 0.16G acceleration was achieved by connecting two modules via a 300-meter tether and rotating them at 1 rpm [67]. O'Neill's 1.8 km radius Stanford torus, spinning at 1 rpm, produced Earth's gravity in space [67]. However, in numerous other examples and proposed solutions, the relationship between rotation and radius is closely interdependent. The centripetal acceleration is inversely related to the tangential velocity when the tangential velocity remains constant, but is directly related when the angular velocity remains constant [68]. Consequently, centrifugation is a valid method for generating partial gravity, which can be as low as 0.001G [69]. However, during centrifugation, it is crucial to rotate the system around its own axis to prevent sedimentation, as shown in [Figure 10](#) [70].

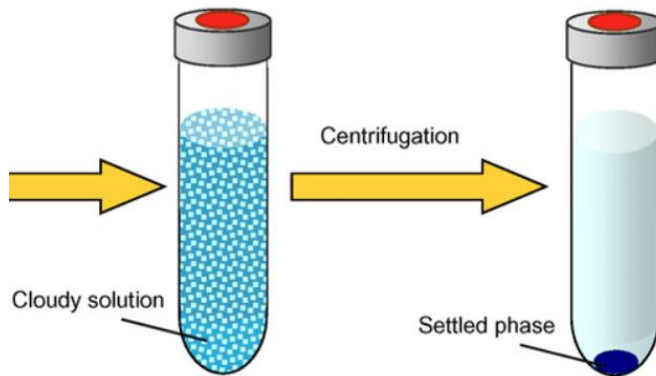


Figure 10. Schematic Diagram of Centrifugation to Settle Particles

The proposed solution emphasizes the ability to use a set of rotating bioreactors tailored to specific gravitational forces. As the system encompasses four distinct gravity levels, the solution entails four separate bioreactors, each stabilized with its own diameter. These bioreactors would feature varying radii, enabling the simulation of partial gravity without subjecting the cells to undue shear stress from rotational motion and friction within the medium. Additionally, each bioreactor would be equipped with its own motor. Regarding the observational equipment, a camera will be positioned to provide a frontal view of all bioreactor surfaces, extending from the base of the prototype in an L-shaped configuration to encompass all units. Figure 11 illustrates the overall design schematic.

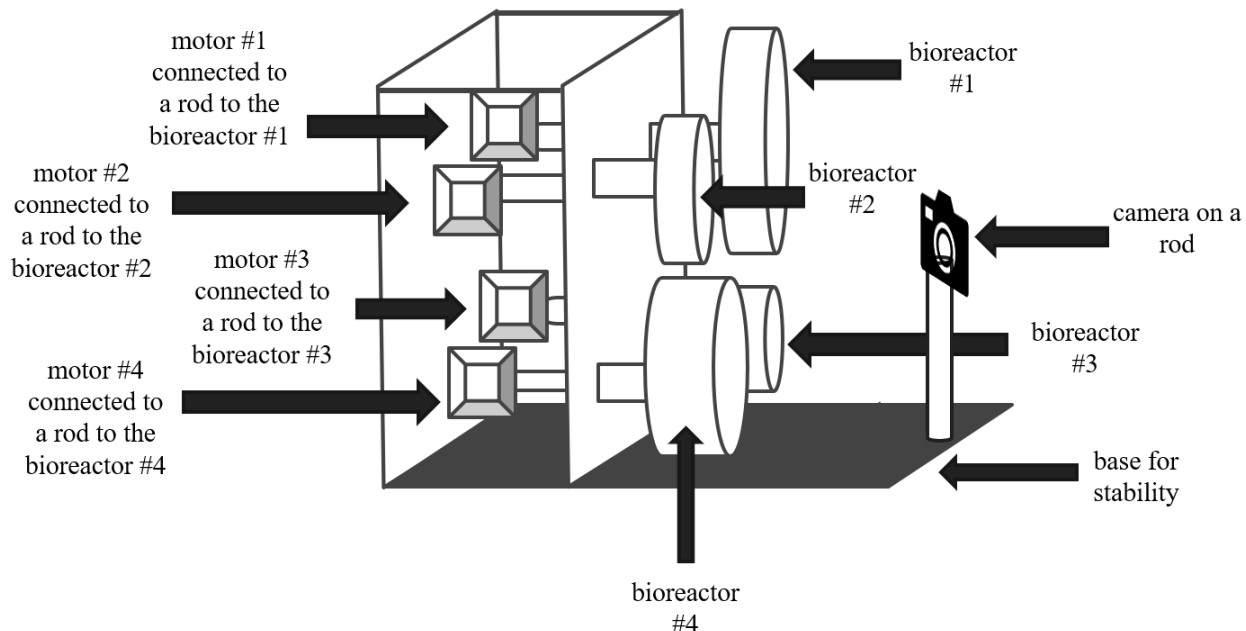


Figure 11. Rough Sketch of the Centrifugation Solution

There are four different bioreactors with different diameters, each attached to a motor. All the bioreactors are held in place by a vertical plane. The camera is placed to view the whole circumference of all the bioreactors.

Solution P.C: Inclined Plane (Single Motor)

This proposed solution outlines the use of an inclined-plane single-motor bioreactor equipped with an integrated camera monitoring system as an innovative approach to enhancing the efficiency of cell culture processes. The system is engineered to optimize mixing, oxygen transfer, and gentle agitation—all vital for the proliferation of cells in suspension under partial gravity conditions. These hydrodynamic parameters can be quantified using specific power input (P/V), which correlates motor power with culture volume and serves as an essential metric to ensure proper mixing while preventing excessive shear forces. By maintaining P/V within the ranges established for mammalian and microbial culture systems, the design aims to balance nutrient and gas transfer requirements while safeguarding sensitive cell cultures [71].

For real-time visualization, the system will incorporate a camera with adjustable focus and LED illumination to ensure uniform brightfield imaging. To maintain consistent image quality during bioreactor operation, the camera shall be mounted directly to the rotating vessel assembly, thereby following the vessel's motion and orientation changes. This methodology ensures the camera maintains a constant field of view relative to the culture. The camera is affixed using a gimbal-like (think of a movable selfie stick) system, which keeps the lens aligned with the observation window throughout the entire range of vessel motion.

The bioreactor's control is handled by a microcontroller platform, such as an Arduino, which regulates motor speed, acquires sensor data, and operates the camera. Data logging facilitates the export of sensor readings and image sequences for subsequent analysis. Safety features include overcurrent protection, temperature cutoffs, and emergency stop mechanisms to ensure the safety of both the vessel and its cultural contents.

The rotation and tilt operation using a single motor effectively facilitates controlled vessel rotation; however, it offers limited flexibility in adjusting the vessel's angle. In the simplest configuration, the motor drives the vessel at a fixed RPM, while the axis of rotation remains stationary; the angle relative to gravity is mechanically preset on the mounting frame. This configuration indicates that the speed and angle cannot be adjusted simultaneously, as the motor can execute only one function at a time. More sophisticated systems, such as differential gears, could be implemented; however, they introduce additional mechanical complexity, thereby reducing overall efficiency [71]. A rough sketch of the solution is seen in [Figure 12](#).

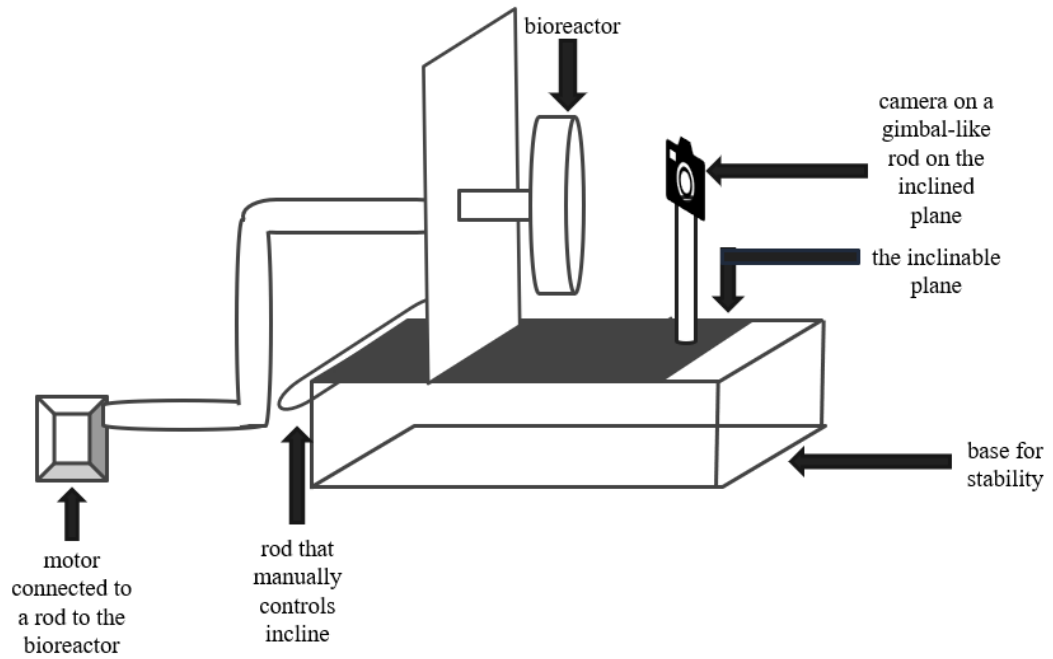


Figure 12. Rough Sketch of Inclined Plane with Single Motor

The figure illustrates the preliminary sketch for the single-motor inclined plane. The bioreactor is connected to the motor via a tube, and the incline plane is adjusted manually.

3.3 Decision Matrix

Selecting the appropriate approach for the bioreactor necessitates evaluating multiple factors, including availability, research utilization, and bubble formation. For the partial gravity scenario, the factors considered are gravitational type, overall device size, and design time. Given that each option has its own advantages and disadvantages, a weighted comparison is essential to identify the optimal solution. A prioritization (weighted decision) matrix is employed to evaluate the options based on predetermined criteria [72].

Regarding the bioreactor, the primary criterion to consider is availability. Since this prototype comprises two components, with a particular emphasis on the partial gravity section, the RWV is expected to have a minimal impact on the project timeline. Consequently, this criterion is assigned a score of 5 points. A score of 1 indicates that the component is either not accessible or requires design development. In contrast, a score of 2 means that it is accessible and requires no additional design effort.

The second criterion pertains to the formation of bubbles. Bubble formation represents one of the most limiting factors in data extraction and is therefore assigned a weight of four points. A rank of one indicates that bubble formation is present or disrupts fluid motion, whereas a rank of two signifies that bubble formation does not interfere with the flow of the medium.

Finally, the third criterion pertains to research utilization: the number of literature papers that have employed the bioreactor. If research articles have utilized the bioreactor and data extraction occurred without issues, this suggests that the bioreactor is appropriate for use, or that its disadvantages do not outweigh its advantages. Given that the primary objective is to employ the bioreactor for research purposes, this criterion is assigned a weight of two points. A ranking of 1 indicates minimal use in literature, whereas a ranking of 2 signifies more widespread application. With these criteria established, the decision matrix is accordingly defined.

Regarding partial gravity, the criteria are gravitational type, overall device size, and design time. The primary criterion concerns the gravitational type (see [Table 1](#)). Since the main objective is to attain $\frac{1}{6}G$, $\frac{3}{8}G$, $1G$, and μG to verify the locations' gravitational properties that NASA is reluctant to explore, the gravitational type criterion is assigned a weight of 5 points [51], [73]. The ranking of this criterion is based on where such gravitational values can be achieved. A rank of 1 indicates that only those four gravity values are achieved, whereas a rank of 3 signifies that more gravitational values can be achieved.

The second criterion concerns the overall device size (see [Table 1](#)). When the device is situated within the incubator, its size is limited by the dimensions of $23 \times 17 \times 14$ in. Nonetheless, due to the design's substantial dependence on the type of bioreactor used and the restrictions on dimension ranking, a score of 2 points is assigned. Consequently, this criterion is assessed based on the likelihood of space utilization, with a ranking of 1 indicating considerable spatial occupation and 3 indicating minimal space consumption.

The final criterion relates to the design timeline. Considering that the project must be completed within three months, the proposed solution must adhere to this schedule. However, due to the materials used in the device's procurement schedules and supply arrival, this criterion shall be assigned a weight of 2 points. The

ranking for this criterion is based on the ease of project replication, with 1 indicating a prolonged or unprecedented process and 3 indicating swift completion. Once the criteria are established, the decision matrix is accordingly identified.

After evaluating the criteria for the bioreactor presented in [Table 3](#), the novel RWV bioreactor received the highest score of 20 points. Consequently, the selected bioreactor is the novel model. Upon assessing the criteria for partial gravity, as shown in [Table 4](#), the inclined plane with dual motors achieved the highest score of 23 points. Therefore, the preferred solution is the novel RWV on an inclined plane with dual motors.

Table 3. Design Matrix for RWV Solutions

Criteria	Weight	Standard RWV		Novel RWV	
		Rating	Weighted Score	Rating	Weighted Score
Availability	5	2	10	2	10
Bubble Formation Disrupts Flow	4	1	4	2	8
Research Usage	2	2	4	1	2
Total Score			18		20

The table displays the criteria and their corresponding weights, which determine the favorable RWV solution. The rating and weighted score for each solution are shown. The novel RWV scored the highest.

Table 4. Design Matrix for Partial Gravity Solutions

Criteria	Weight	Inclined Plane with Dual Motor		Four Centrifugations		Inclined Plane with One Motor	
		Rating	Weighted Score	Rating	Weighted Score	Rating	Weighted Score
Gravitational Type	5	3	15	1	5	2	10
Dimensions	2	1	2	3	6	2	4
Design Time	2	3	6	2	4	1	2
Total Score			23		15		16

The table shows the criteria and their weights, which determine the favorable partial gravity solution. The rating and weighted score for each solution are displayed. The inclined plane with dual motors scored the highest.

4. Engineering Design

The engineering design of the solution is founded on detailed methodologies, calculations, and components to facilitate the successful execution of the partial gravity applied to the cells. This section outlines the theory, calculations, and mechanical design

materials, electronics, and validation strategies used to confirm that the selected options meet the system requirements.

4.1 Design Rationale

According to the most essential non-negotiable criteria, the prototype should have the ability to induce at least four different gravitational types: $1G$, $\frac{3}{8}G$, $\frac{1}{6}G$, and μG . To simulate partial gravity on Earth, various methods, such as parabolic flight, centrifugation, or modified rotation devices, could be used [74].

The parabolic flight methodology enables researchers to conduct experiments in microgravity and partial gravity, thereby simulating lunar or Martian environments in line with NASA's mission objective to facilitate human space exploration [75]. The technique utilized to recreate these conditions involves controlled maneuvers that temporarily induce free fall through the following procedures: pull-up, wherein the aircraft ascends at a steep angle (45°) enabling passengers to experience $1.8G$; push-over, whereby, upon reaching the apex of the parabolic arc, the pilot reduces engine thrust, causing all objects inside the aircraft to descend together; reduced gravity, which occurs during the descent when no force acts upon the occupants, creating weightless conditions similar to those in space; and pull-out, where increased engine thrust and leveling out return the aircraft to Earth's gravity [75]. However, this approach has several limitations, including the short duration of reduced gravity, approximately 20 seconds per parabola, with typical flights comprising between 15 and 30 parabolas [75].

Centrifugation is employed to modify the magnitude of Earth's gravitational force in accordance with Einstein's Equivalence Principle, demonstrating that there exists no physical distinction between acceleration due to mass and linear acceleration [76], [77]. Operating a centrifuge at a constant velocity allows the sample to change direction and remain centered during rotation continually [77]. Recognizing that the inertia of the sample and the rotation of the centrifuge collectively generate gravitational effects, the magnitude of this simulated gravity is dependent on the radius of the centrifuge and its angular velocity [77]. Centrifuges are used to mimic microgravity conditions through the Reduced Gravity Paradigm (RGP), which emphasizes responses to the difference between two levels of acceleration [77]. RGP is most effective when applied to a stable and steady system operating at a high gravitational level before reducing the acceleration [77]. Optimal results are observed in systems that respond rapidly; intermediate- and slow-responding systems require more time than the available time interval to achieve the desired gravity level [77].

Given the importance of stability in centrifugation, modified rotational devices, including bioreactors, are evaluated for their efficacy in partial-gravity simulation. Bioreactors are biomechanically active systems engineered to replicate biological conditions by utilizing mechanical means to influence cellular processes

through the meticulous regulation of biochemical and physical signals [78]. RWV, which employs vessel rotation to generate low-shear mixing and simulated microgravity within the chamber, is available in two variants: the slow-turning lateral vessel (STLV) and the high-aspect-ratio vessel (HARV), as illustrated in [Figure 13](#) [79]. The differences between these two types include the fact that STLVs incorporate a central cylinder oxygenator and can accommodate larger volumes. In contrast, HARVs are equipped with a gas-permeable member on one of their walls to enhance oxygenation [79].

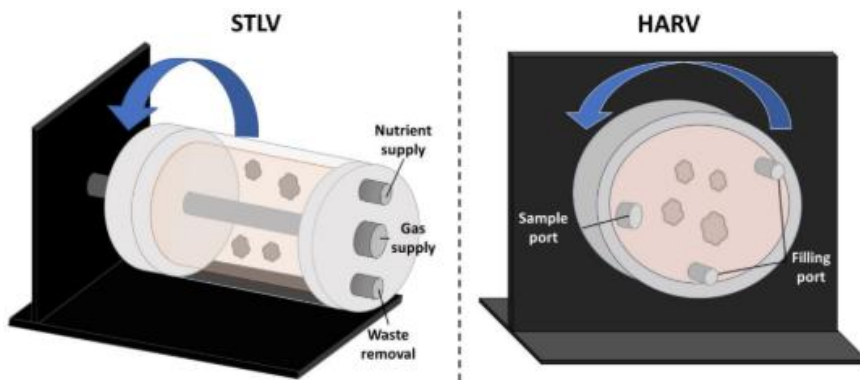
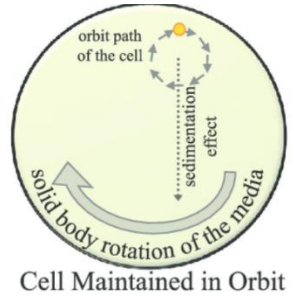


Figure 13. Spherical Tissue Lateral Vessel (STLV) vs High Aspect Ratio Vessel (HARV)

The figure on the left depicts the Spherical Tissue Lateral Vessel (STLV) bioreactor, with its ports labeled. To the right, the HARV is displayed, also with labeled ports. A cylindrical shape characterizes the Spherical Tissue Lateral Vessel, whereas the HARV has a disc-shaped configuration [79].

Despite the limitations associated with the RWV, which include the requirement for high user competency, bubble formation, and the difficulty in determining the appropriate rotational speed to balance solid-body rotation with continuous freefall, the device enhances cellular performance through its capacity to improve mixing in low-shear environments substantially, facilitate high-density cell cultures and self-aggregation, promote cellular differentiation, and, notably, simulate microgravity [80], [81]. The effects of this simulation are well documented, encompassing alterations in calcium handling within cardiac cells and interference with cellular differentiation pathways [82].

The proposed solution emphasizes integrating the benefits of different types of partial gravity simulation while minimizing adverse effects. To optimize cell growth, it is essential to cultivate cells in a manner that simulates free-fall. Consequently, maintaining a constant and steady rotation of the cells is necessary to ensure continuous exposure to free-fall conditions. This objective can be achieved by modifying RWV rotation through the integration of centrifugation methods. As depicted in [Figure 14](#), the device's orbit will be controlled to maintain a low-shear environment, with balanced solid-body rotation and continuous free-fall conditions [83].



Cell Maintained in Orbit

Figure 14. Orbit Trajectory of the Cell Within a Rotating Bioreactor

The orbital trajectory of the cell within a rotating bioreactor. The sustained rotation and sedimentation effects prevent the cells from settling at the base of the vessel. Additionally, the clockwise rotation of the medium facilitates the continuous suspension of cells in the orbit [83].

However, the centrifugation process would not accurately simulate the partial gravity of $\frac{1}{6}G$ and $\frac{3}{8}G$, without affecting cell viability. With the inclination in parabolic flight enabling a 1.8G simulation, the inclined plane in the solution would serve as the primary mechanism for achieving partial gravity conditions. In fact, NASA is presently constructing a Mars Artificial Gravity Habitat with Centrifugation (MAGICIAN) module to emulate Earth's gravity on Mars, as illustrated in [Figure 15](#) [84].

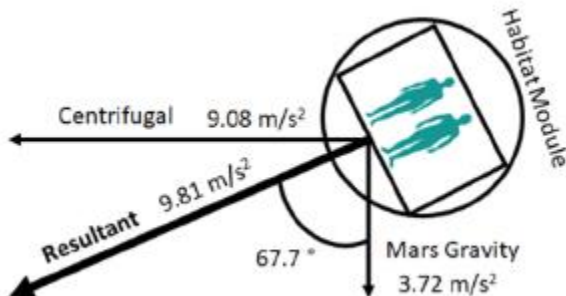


Figure 15. MAGAICIAN Schematic

A two-dimensional cross-section of the MAGIGAN modules displayed at an angle of 67.7° to achieve a resultant force equivalent to Earth's gravity [84].

Using a bioreactor would provide a controlled environment for cell growth, thereby reducing the likelihood of inaccurate data resulting from cell culture. Given that the bioreactor's rotation is maintained at a constant rate and the inclined plane's movement is solely a result of gravitational simulation, two motors will be employed.

4.2 Calculations

To construct the prototype, specific calculations must be performed. These calculations will be utilized for simulation purposes to validate the prototype. To generalize the calculation, the specimen will be referred to as a particle; however, this term also applies to cells and the samples used during validation.

Incline Plane

The inclined plane facilitates the reduction of the gravitational force exerted on a particle by decomposing it into components. Referring to Figure 16, the gravitational force is entirely on one axis (when $\theta^{\circ} = 0^{\circ}$ or 90°) or decomposed into components. Utilizing trigonometry, Eq. 2 and Eq. 3 illustrate the values for the parallel and perpendicular components of gravity relative to the plane [85].

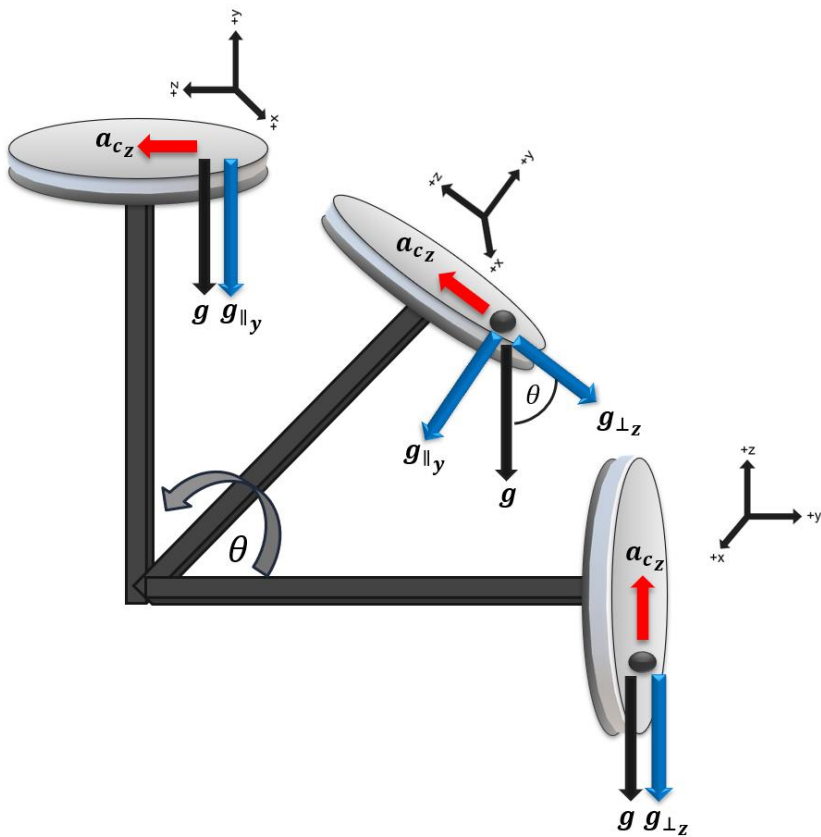


Figure 16. Free Body Diagram of a Bioreactor on an Inclined Plane

When the plane is parallel to the base, the gravitational force acts in the z-direction. When the plane is inclined at an angle θ from the base, the gravitational force is resolved into components. When the plane is perpendicular to the base, the gravitational force acts in the y-direction. The blue arrows represent the components of the gravity present in each scenario.

$$g_{\parallel y} = g \sin \theta^{\circ} \quad (2)$$

Equation 2. Parallel Gravitational Component

Where:

$g_{\parallel y}$ = gravitational component parallel to the plane

g = Earth's gravity ($9.81 \frac{m}{s^2}$)

θ° = angle between the inclined plane and the base

$$g_{\perp z} = g \cos \theta^\circ \quad (3)$$

Equation 3. Perpendicular Gravitational Component (Tangential Gravity)

Where:

$g_{\perp z}$ = gravitational component perpendicular to the plane

g = Earth's gravity ($9.81 \frac{m}{s^2}$)

θ° = angle between the inclined plane and the base

Since the bioreactor remains stable along the y-axis, meaning it does not slide on the inclined plane, $g_{\parallel y}$ is the effective gravitational force due to this stability, seen in Eq. 4. This is because the centripetal acceleration lies in the yz-plane, meaning the bioreactor rotates around the y-axis. Regarding, it is aligned with the axis of centripetal acceleration, making $g_{\perp z}$ the gravitational component that balances the rotational acceleration. Centripetal acceleration will be used instead of centrifugal acceleration because the particle's position is ideal in the middle of the bioreactor (not near its circumference). Solving Eq. 2 for in terms of θ , Eq. 5 shows the angle of the inclined plane that produces the effective gravitational force.

$$\begin{aligned} g_{tar} &= g_{\parallel y} \\ g_{tar} &= g \sin \theta^\circ \end{aligned} \quad (4)$$

Equation 4. Targeted Gravity Case 1

Where:

g_{tar} = intended partial gravity

$g_{\parallel y}$ = gravitational component parallel to the plane

g = Earth's gravity ($9.81 \frac{m}{s^2}$)

θ° = angle between the inclined plane and the base

$$\theta = \sin^{-1}\left(\frac{g_{\parallel y}}{g}\right) \quad (5)$$

Equation 5. Inclined Plane Angle

Where:

g_{tar} = intended partial gravity

$g_{\parallel y}$ = gravitational component parallel to the plane

g = Earth's gravity ($9.81 \frac{m}{s^2}$)

θ° = angle between the inclined plane and the base

Although the inclination angle equation establishes the environment in which the particle experiences modified gravitational forces, the particles should be in a state of "free fall" at any inclination position. Therefore, calculating the centripetal acceleration is necessary.

Centripetal Acceleration

Given that uniform, steady circular motion is required for laminar flow, centripetal acceleration will be used. The centripetal acceleration (a_c) is directed towards the center, with the sole opposing acceleration being $g_{\perp z}$. Therefore, the accelerations should be counteracting to ensure that no net force is exerted on the particle, as demonstrated in Eq. 6, with Eq. 3 and the substitution of the relevant quantities for a_c .

$$a_c = g_{\perp z} \Rightarrow \\ \omega^2 R = g \cos \theta^\circ \quad (6)$$

Equation 6. Net Horizontal Acceleration

Where:

a_c = centripetal acceleration

$g_{\perp z}$ = gravitational component perpendicular to the plane

ω = angular velocity

g = Earth's gravity ($9.81 \frac{m}{s^2}$)

θ° = angle between the inclined plane and the base

R = radius of rotation of the particle to the center

The preceding steps are predicated on the initial assumption that the component of gravity parallel to the plane constitutes the target of partial gravity, as seen in Eq. 4, with the perpendicular component aligned along the same axis as the centripetal acceleration, thereby facilitating cancellation. Nonetheless, during circular motion, the particle does not remain fixed at a single position; instead, it encounters varying net accelerations at different locations. Consequently, two additional positions are calculated to determine the

necessary RPM range. Previously, it was assumed that the particle was moving only along one axis, as illustrated in [Figure 16](#). For the positions of interest, it assumes that all accelerations acting on the particle will partially cancel each other out until the desired net acceleration is achieved. This total acceleration is denoted as g_{tar} , where it stands for the intended partial gravity.

[Eq. 7](#) shows the total gravity calculated from the free-body diagrams when the particle is at the top and the bottom.

$$g_{tar} = \sqrt{(\omega^2 R \pm g_{\perp z})^2 + g_{\parallel y}^2} \quad (7)$$

Equation 7. Targeted Gravity in Top and Bottom Placement

Where:

ω = angular velocity

R = radius of bioreactor

g_{tar} = intended partial gravity

$g_{\parallel y}$ = gravitational component parallel to the plane

$g_{\perp z}$ = gravitational component perpendicular to the plane

As for the sides, the particle will have the equation shown in [Eq. 8](#).

$$g_{tar} = \sqrt{(\omega^2 R)^2 + g_{\perp z}^2 + g_{\parallel y}^2} \quad (8)$$

Equation 8. Targeted Gravity in Sides Placement

Where:

ω = angular velocity

R = radius of bioreactor

g_{tar} = intended partial gravity

$g_{\parallel y}$ = gravitational component parallel to the plane

$g_{\perp z}$ = gravitational component perpendicular to the plane

Being less detailed on the vector location and using the cosine rule, the intended partial gravity can also be calculated as seen in [Eq. 9](#). However, in this equation, the angling of the plane does not have an effect.

$$g_{tar} = \sqrt{(\omega^2 R)^2 + g^2 + 2 * g * \omega^2 R * \cos \alpha^\circ} \quad (9)$$

Equation 9. Targeted Gravity in Overall Placement

Where:

ω = angular velocity

R = radius of bioreactor

g_{tar} = intended partial gravity

g = Earth's gravity ($9.81 \frac{m}{s^2}$)

α = angle between the gravity vector and the centripetal acceleration vector

Using Eq. 6 and solving for the centripetal acceleration in Eqs . 6, 7, 8, and 9, the centripetal acceleration at different positions of the system is given in Eq. 10.

$$\begin{aligned} a_c &= g \cos \theta^\circ \\ a_c &= \sqrt{g_{tar}^2 - g_{\parallel y}^2} \pm g_{\perp z} \\ a_c &= \sqrt{g_{tar}^2 - g_{\parallel y}^2 - g_{\perp z}^2} \\ a_c &= -g * \cos \alpha^\circ \pm \sqrt{g_{tar}^2 - g^2 * \sin^2 \alpha^\circ} \end{aligned} \quad (10)$$

Equation 10. Centripetal Acceleration

Where:

a_c = centripetal acceleration

g = Earth's gravity ($9.81 \frac{m}{s^2}$)

θ° = angle between the inclined plane and the base

g_{tar} = intended partial gravity

$g_{\parallel y}$ = gravitational component parallel to the plane

$g_{\perp z}$ = gravitational component perpendicular to the plane

α = angle between the gravity vector and the centripetal acceleration vector

Following the establishment of the connection for a_c , ω can be subsequently calculated.

Angular Velocity

After manipulating Eq. 6, Eq. 11 was used to isolate the angular velocity.

$$\omega = \sqrt{\frac{a_c}{R}} \quad (11)$$

Equation 11. Angular Velocity

Where:

ω = angular velocity

a_c = centripetal acceleration

R = radius of rotation of the particle to the center

RPM

Utilizing Eq. 12, the relationship between RPM and angular velocity is demonstrated [86].

$$RPM = \frac{60\omega}{2\pi} \quad (12)$$

Equation 12. RPM

Where:

RPM = revolutions per minute

ω = angular velocity

Substituting Eq. 11 into Eq. 12, Eq. 13 shows the RPM for the bioreactor.

$$RPM = \frac{60}{2\pi} \sqrt{\frac{a_c}{R}} \quad (13)$$

Equation 13. Bioreactor RPM

Where:

RPM = revolutions per minute

a_c = centripetal acceleration

R = radius of rotation of the particle to the center

The bioreactor's rotation could subsequently be calculated. However, one of the limiting factors in its rotation is the linear velocity induced by the fluid's tangential motion. Therefore, it is necessary to determine the system's linear velocity.

Linear Velocity

The fluid within the bioreactor exhibits tangential movement concurrent with rotation. Eq. 14 illustrates the relationship between angular velocity and linear velocity [86].

$$v = \omega R \quad (14)$$

Equation 14. Linear Velocity in Terms of Angular Velocity

Where:

ω = angular velocity

v = linear velocity

R = radius of rotation of the particle to the center

By substituting Eq. 11 into Eq. 3, Eq. 15 illustrates the linear velocity of the bioreactor.

$$v_{\perp} = \sqrt{R * a_c} \quad (15)$$

Equation 15. Tangential Velocity

Where:

v_{\perp} = tangential velocity

a_c = centripetal acceleration

R = radius of rotation of the particle to the center

Given that the fluid possesses a tangential velocity, the particles suspended within it exhibit a sedimentation velocity. To facilitate "free-fall" conditions for the particles, the sedimentation velocity must be computed.

Sedimentation Velocity

Sedimentation velocity refers to the terminal velocity of a particle within a quiescent fluid [87]. At this velocity, the particle experiences no acceleration because its terminal velocity remains constant. Utilizing Stokes's law, the upward drag force resisting the particle's descent must be equal to the downward gravitational force [88]. However, Stokes's law is predicated upon three fundamental assumptions:

- 1) The particle is small and spherical.
- 2) The particle does not rotate within the fluid.
- 3) Reynold's number is considerably less than 1.

Although cells are not perfectly spherical, Stokes' law provides an approximate estimation of the terminal velocity. For simplification purposes, the extraction of the equation would be visualized in a 2D system. Referring to [Figure 17](#), the particle is suspended within the fluid; therefore, the net force exerted on the particle can be calculated as shown in Eq. 16.

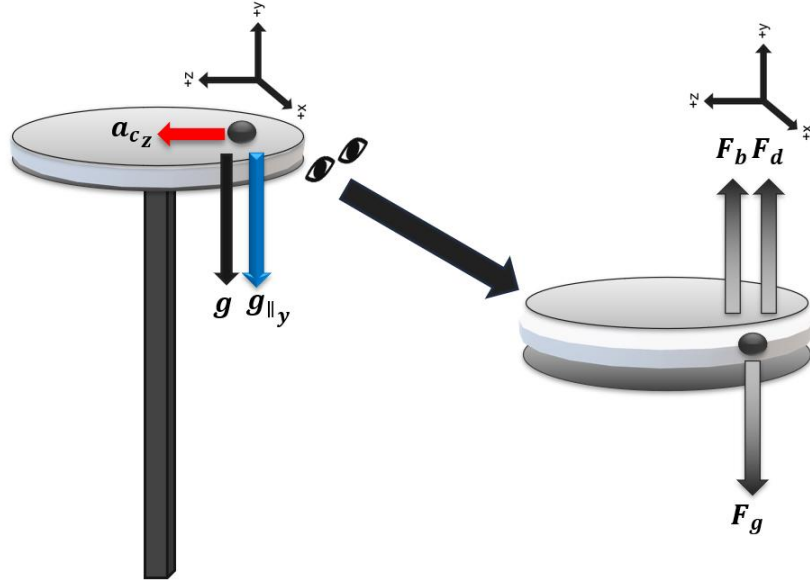


Figure 17. Free Body Diagram of the Particle in Fluid

The figure illustrates the forces acting upon the particle during its suspension within the fluid.

$$F_g = F_b + F_d \quad (16)$$

Equation 16. Net Driving Force on the Particle

Where:

F_g = gravitational force exerted on the particle (the gravitational component that causes the fall)

F_b = buoyancy force exerted on the particle

F_d = drag force exerted on the particle

Eq. 17 and Eq. 18 show the equivalence of the gravitational force (F_g) in a fluid and the buoyancy force (F_b), respectively [88].

$$F_g = V * \rho_p * g_{tar} \quad (17)$$

Equation 17: Equivalence of Gravitational Force

Where:

F_g = gravitational force exerted on the particle

V = volume of the particle

ρ_p = density of the particle

g_{tar} = intended partial gravity

$$F_b = V * \rho_f * g_{tar} \quad (18)$$

Equation 18: Equivalence of Buoyancy Force

Where:

- F_g = gravitational force exerted on the particle
- V = volume of the particle
- ρ_f = density of the fluid
- g_{tar} = intended partial gravity

Assuming that the particle's shape is spherical, the volume of the sphere is determined as shown in Eq. 19.

$$V_s = \frac{4}{3}\pi r^3 \quad (19)$$

Equation 19: Volume of Sphere

Where:

- V_s = volume of the sphere
- r = radius of the sphere

The drag force under consideration is that exerted on a spherical particle, as demonstrated in Eq. 20 [88].

$$F_d = 6\pi r \eta_f v_t \quad (20)$$

Equation 20: Drag Force

Where:

- F_d = drag force exerted on the particle
- r = radius of the particle
- η_f = fluid viscosity
- v_t = sedimentation velocity

Utilizing Eqs. 17-20, Eq. 21 is derived as the fully substituted form of Eq. 16.

$$\begin{aligned} F_g &= F_b + F_d \Rightarrow \\ V_s * \rho_p * g_{tar} &= V_s * \rho_f * g_{tar} + 6\pi r \eta_f v_t \Rightarrow \\ \frac{4}{3}\pi r^3 * \rho_p * g_{tar} &= \frac{4}{3}\pi r^3 * \rho_f * g_{tar} + 6\pi r \eta_f v_t \end{aligned} \quad (21)$$

Equation 21: Fully Derived Net Driving Force on the Particle

Where:

- r = radius of the particle
- ρ_p = density of the particle
- ρ_f = density of the fluid
- g_{tar} = intended partial gravity
- η_f = fluid viscosity
- v_t = sedimentation velocity

The sedimentation velocity equation, as seen in Eq. 22, is derived from Eq. 21 [88].

$$v_t = \frac{2}{9\eta_f} (\rho_p - \rho_f) * r^2 * g_{tar} \quad (22)$$

Equation 22: Sedimentation Velocity

Where:

- v_t = sedimentation velocity
- r = radius of the particle
- ρ_p = density of the particle
- g_{tar} = intended partial gravity
- ρ_f = density of the fluid
- η_f = fluid viscosity

Nevertheless, the values derived from the settling velocity are predicated upon various assumptions. To confirm that the particle remains in laminar flow, thereby validating the preceding calculations of sedimentation velocity, the Reynolds number (Re_p) should be computed [88]. The particle Reynolds number should be less than 2,000 to maintain laminar flow. If it exceeds 3,500, the flow becomes turbulent; for values in between, the flow is transitional [89]. By utilizing Eq. 23, these calculations can be confirmed [90].

$$Re_p = \frac{\rho_f * (v_p + v_f) * 2 * r}{\eta_f} < 2,000 \quad (23)$$

Equation 23. Particle Reynolds Number

Where:

- Re_p = particle Reynolds number
- ρ_f = density of the fluid
- v_f = velocity of the fluid
- v_p = velocity of the particle
- r = radius of the particle
- η_f = fluid viscosity

Given the presence of motion, shear stress influences both the particle and the fluid. Shear stress is defined as the deformation of an object due to the application of a tangential force on its surface [91]. The maximum shear stress on the particle occurs at the circumference, as indicated by Eq. 24, which demonstrates the maximum shear stress on the particle [90].

$$\tau_{max} = \mu \frac{v_t^3}{2r} \quad (24)$$

Equation 24. Particle Shear Stress

Where

v_t = sedimentation velocity

τ_{max} = maximum shear stress

μ = fluidic dynamic viscosity

r = radius of the particle

Regarding the fluid shear stress, it originates from laminar flow, resulting in varying fluid velocities at different levels [92]. Shear stress within the fluid can influence cellular integrity to such an extent that it may induce cell death [92]. Eq. 25 delineates the shear stress exerted by a Newtonian fluid on a surface [93]. This equation may be applicable in modeling the interaction between bubbles and particles [64].

$$\tau = \mu \frac{\partial v}{\partial r} \quad (25)$$

Equation 25. Fluid Shear Stress

Where

τ = fluid shear stress

μ = fluidic dynamic viscosity

$\frac{\partial v}{\partial r}$ = gradient of the fluidic velocity (shear rate)

Given that the fluid undergoes continuous rotation, the velocity gradient can be approximated by the system's tangential velocity. Furthermore, since the initial simulation and calculations primarily focus on the maximum shear in all cases, the change in radius would not occur, implying that the radius remains the same. Accordingly, Eq. 25 can be expressed as shown in Eq. 26.

$$\tau = \mu * \omega R \quad (26)$$

Equation 26. Fluid Shear Stress

Where

τ = fluid shear stress

μ = fluidic dynamic viscosity

ω = angular velocity

R = radius of rotation of the particle to the center

With further comprehensive research, the shear stress could achieve higher accuracy. However, several experimental tests were conducted using a cylinder instead of a disc to measure the wall shear stress of specific fluids. Since there are no numerical values, the shear stress would be calculated using an expected RPM and adjusted until the acceptable shear stress is calculated.

Dynamic Portion

To improve the mathematical model and obtain more precise RPM values, certain factors influenced by rotational effects must be considered. Cells undergo continuous growth during culture, which affects the number of particles in the bioreactor. Consequently, the progression of cell growth over time is a critical factor. Although various models describe cell growth, the exponential growth model will be employed to simulate the most extreme scenario, as defined by Eq. 27 [94].

$$N(t) = N_o e^{rt} \quad (27)$$

Equation 27. Particle Growth Over Time

Where:

$N(t)$ = particle concentration over time

N_o = initial particle concentration

t = time (in hours)

r = population growth rate

Since particles act as barriers within fluids, increasing particle concentration increases viscosity [95]. Using the model developed by Krieger and Dougherty, this impact on viscosity can be quantified. Eq. 28 shows the relevant equation for both low and high shear rates [95]. Assuming the particles are spherical, the maximum packing density is approximately 0.648, and the intrinsic viscosity is 2.5 [95].

$$\eta_{f,n} = \eta_f \left(1 - \frac{\phi}{\phi_{max}}\right)^{-[\eta]*\phi_{max}} \quad (28)$$

Equation 28. Viscosity Change

Where:

$\eta_{f,n}$ = altered fluid viscosity

η_f = fluid viscosity initial (before adding particles)

ϕ = solid fraction in suspension

ϕ_{max} = maximum solid fraction in the suspension

$[\eta]$ = intrinsic viscosity that is dependent on particle shape

As the particle concentration increases, the solid fraction in suspension (ϕ) will change over time. Eq. 29 illustrates the variation of the solid fraction [95].

$$\phi(t) = \frac{N(t)*V_p}{V_f} \quad (29)$$

Equation 29. Dynamic Solid Fraction in Suspension

Where:

$\phi(t)$ = solid fraction in suspension (dynamic)

$N(t)$ = particle concentration over time

V_p = volume of one particle

V_f = volume of fluid

The viscosity change would then be dynamic, as seen in Eq. 30.

$$\eta_{f,n}(t) = \eta_f(1 - \frac{\phi(t)}{\phi_{max}})^{-[\eta]*\phi_{max}} \quad (30)$$

Equation 30. Dynamic Viscosity Change

Where:

$\eta_{f,n}$ = altered fluid viscosity

η_f = fluid viscosity initial (before adding particles)

$\phi(t)$ = solid fraction in suspension (dynamic)

ϕ_{max} = maximum solid fraction in the suspension

$[\eta]$ = intrinsic viscosity that is dependent on particle shape

Eq. 26 accounts for fluid shear stress and dynamic viscosity. As shown in Eqs. 29 and 30, changes in particle concentration result in variations in fluid viscosity. Additionally, to maintain the system's integrity and prevent particle failure or death, the rotational velocity must be adjusted appropriately. Therefore, using Eqs. 26 and 30, Equation 31 depicts the dynamic fluid shear stress.

$$\tau(t) = \eta_{f,n}(t) * \omega(t)R \quad (31)$$

Equation 31. Dynamic Fluid Shear Stress

Where

$\tau(t)$ = fluid shear stress (dynamic)

$\eta_{f,n}(t)$ = altered fluid viscosity (dynamic)

$\omega(t)$ = angular velocity (dynamic)

R = radius of rotation of the particle to the center

As particle properties change over time, the RPM needs to be adjusted to counteract the relevant gravity component. However, the current mathematical model lacks sufficient detail for precise accuracy, leading to an overestimation of RPM. Therefore, the RPM would be selected and fine-tuned based on particle property limits, such as maximum shear stress.

4.3 Numerical Sampling

As mentioned in the [Calculations - Centripetal Acceleration Section](#), three methods were used to calculate the RPM and the angle required to achieve the desired gravity. From the calculations, some imaginary values appeared in certain portions, indicating that it would not be realistic to achieve the intended gravity at this location. Additionally, due to vector balancing, some positions resulted in high RPM values. However, to ensure that the particles (specifically the cells) are not harmed by rotation-induced motion, we will use the average RPM and angle for each intended gravity, as shown in [Table 5](#).

Table 5. Numerical Values of Initial RPM and Angle Values

Gravity ($\frac{m}{s^2}$)	Inclined Angle (°)	RPM ($\frac{rev}{min}$)
1G	90°	0
$\frac{3}{8}G$	16°	10
$\frac{1}{6}G$	13°	16
μG	0°	23

The table presents some of the final numerical values derived from the equations detailed in the [Calculation section](#). The table includes four different gravity values and their respective incline angles, along with the RPM for a specific bioreactor radius of 0.025m.

Correlation and Analysis

After calculating both the sedimentation velocity and the tangential velocity, the ratio of these velocities provides valuable insights into particle interactions within the fluid. If the sedimentation velocity exceeds the tangential velocity, the particles will settle, which is undesirable. Conversely, if the terminal velocity is lower than the tangential velocity, the particles remain in suspension continuously. The objective is to ensure that the tangential velocity exceeds the terminal velocity. The correlation is

$$v_t > \approx v_{\perp}$$

If this condition is not satisfied, adjustments to the system should be implemented, such as increasing or decreasing the RPM.

[Figure 18](#) illustrates the correlation between the RPM and the radius. The correlation is

$$RPM \propto \frac{1}{\sqrt{R}}$$

, considering the centripetal acceleration is kept constant. Therefore, as the radius increases, the RPM decreases.

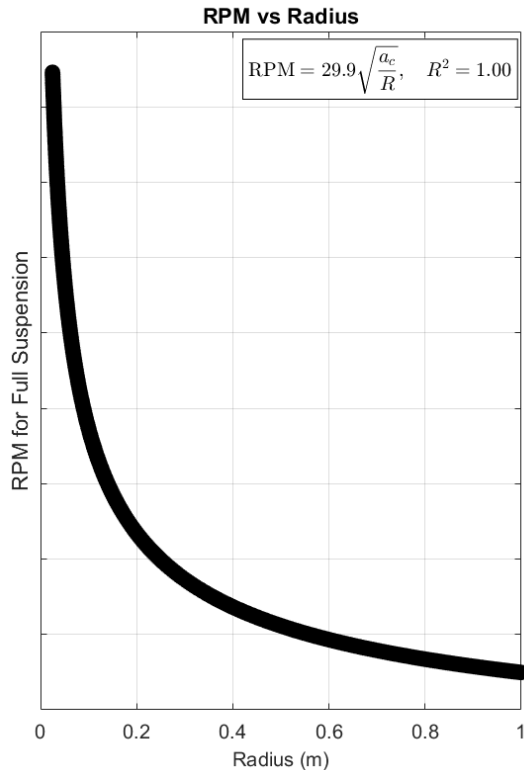


Figure 18. RPM vs Radius

The figure illustrates that increasing the bioreactor radius decreases RPM.

4.4 Simulation

Given the presence of a few mathematical equations, a simulation can be conducted.

Mathematical Simulation

The mathematical simulation relies on the equations presented in the [Calculation](#) section. Since there are many mathematical variables to add to make particle simulations truly accurate, the program was designed to allow easy data addition.

First, the program was done in Python, and four different Python files were created. The files included the following: generalized bioreactor, particle properties, particles in the bioreactor, and the application. The generalized bioreactor file contains functions that either find RPM and tilt from the intended gravity

or, conversely, find the gravity from RPM and tilt. The particle properties (as stated in the [Calculations](#) section) are added to their own functions, each with its own variables, including the dynamic portion. Since the particles will be rotating inside the bioreactor, the ratio of sedimentation velocity to linear velocity is calculated to ensure that particles do not settle and that the shear stress remains within the acceptable range. Additionally, a heatmap showing gravity at each position in the bioreactor is shown, for both perpendicular and parallel gravity. Finally, the application file calls all the functions from the previous files to have an interactive website.

In the application, there are two tabs: simulation and math. The math tab explains the mathematical methods used in this paper and provides a quick summary of the application's mathematical methods. The simulation portion contains the generalized and particle gravities. With that, the application is generated.

The heatmaps show how gravity is felt inside the bioreactor. In [Figure 19](#), the parallel gravity in two different gravity environments (Earth and Mars) is shown. Looking at Earth's gravity, there is a slight color gradient, showing that the gravity is not significantly different from one position to another. However, looking at Mars' gravity, the color gradient varies with the particle's position. As seen in [Figure 19B](#), the bottom area has the lowest gravity, while the top area has the most extreme gravity. The sides have the middle (most accurately intended gravity). This is due to the correlation between RPM and radius, as seen in [Figure 13](#).

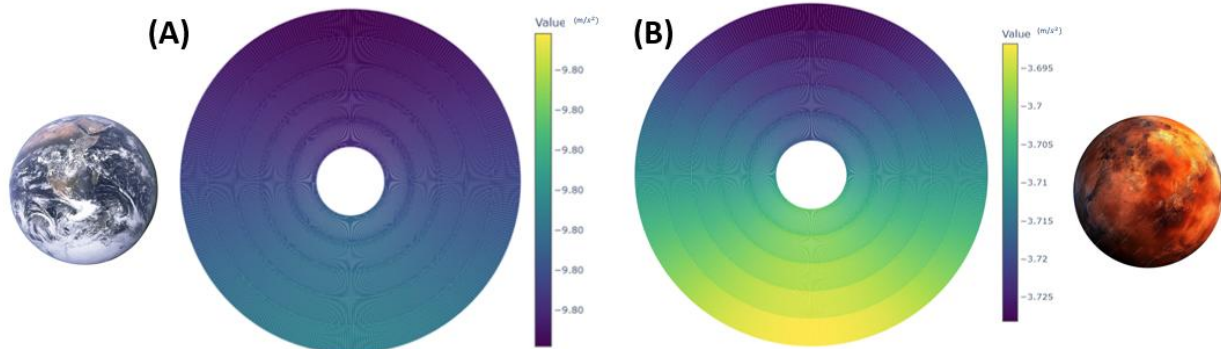


Figure 19: Parallel Gravity Component for Earth and Mars

The figure shows the effective gravity of (A) Earth and (B) Mars inside the bioreactor.

5. Components

After understanding the system's basic operation, choosing the right components is essential.

5.1 Motor, Driver, and Microcontroller

Given that a maximum of 1300 rpm is considered extreme when sustained for more than 10 minutes, as exceeding this limit can result in cell denaturation, a smaller radius is preferable to maintain healthy cell cultures [96]. Regarding view clearance, a significant aspect of the prototype is the visual assessment of the particle under rotation and at different inclinations. Therefore, the chosen bioreactor should have a small radius and a large viewing area.

To determine the torque required to continuously rotate the bioreactor, the moment of inertia and the angular acceleration must be calculated. However, since the bioreactor is expected to rotate from 0 rpm to a maximum of 50 rpm, the angular acceleration can be observed as the intended rpm increases over time. Since RPM provides more information than angular velocity, the torque can be found as seen in Eq. 32 [97].

$$\begin{aligned}\tau &= I * \alpha \Rightarrow \\ \tau &= I * \frac{\Delta\omega}{t} \Rightarrow \\ \tau &= I * \frac{\frac{2\pi}{60} * RPM}{t}\end{aligned}\tag{32}$$

Equation 32. Torque

Where:

τ = torque

α = angular acceleration

ω = angular velocity

RPM = revolution per minute

t = time it takes to change angular velocity

Focusing on the moment of inertia, the bioreactor is a cylinder with some extrusions. Assuming that the bioreactor is a cylinder, the moment of inertia is in Eq. 33 [98].

$$I = \frac{m * r^2}{2}\tag{33}$$

Equation 33. Moment of Inertia

Where:

m = mass of the rotating object

r = radius of the rotating object

I = moment of inertia

Eq. 33 is the inertia of the rotation along the length of the cylinder, which applies to both the bioreactor and the rod. For the bioreactor, the radius would be the 50mL HARV to achieve the most extreme moment of inertia possible for the prototype. A diameter of 99.06mm, corresponding to a radius of 0.04953m, will be used. As for the mass, it was documented from the prior team that the empty mass of the bioreactor is .03kg, and using the volume of 50mL, the density of the water $1,000 \frac{kg}{m^3}$, and the prior knowledge of $1mL = 10^{-6}m^3$ the mass of the filled bioreactor can be measured using Eq. 34 [99].

$$m = \rho * V \quad (34)$$

Equation 34. Mass

Where:

m = mass of the system

V = volume of the system

ρ = density of the system

Adding the mass of the bioreactor to the mass of the system inside it, the mass of the filled bioreactor is 0.08kg. However, since the actual mass of the total bioreactor is never precisely known, a safety factor of 1.5 is used. For that, the mass of the filled bioreactor is 0.12kg. Plugging the filled mass of the bioreactor and the radius of 0.04953m in Eq. 33, the moment of inertia is $1.47 \times 10^{-4} kgm^2$. If it takes 1 second to go from 0 RPM to a maximum RPM of 50 RPM, plugging the values into Eq. 32 will provide a torque of $2.57 \times 10^{-5} \frac{rev}{s^2}$, which is $1.61 \times 10^{-4} Nm$.

Since the torque is very low, most motors would be suitable for the prototype. However, the accuracy of motor rotation at 20-50rpm is essential. Therefore, the best way to achieve that is to break down the steps per motor revolution. The NEMA 17 has a step angle of 1.8° , requiring 200 steps to complete one full turn [100]. It draws up a current phase of 1.6A, and the digital stepper driver used has a current per phase of 0.3-2.2A [100], [101]. Since the current per phase of the motor is within the driver's range, the driver would be applicable. It reaches a maximum temperature of 50 °C, exceeding the incubator's temperature limit. Furthermore, the maximum step resolution is 1/100, allowing the driver to divide a complete step into 100 smaller steps. This enhances the variation in angle increments in the prototype, thereby enabling a broader range of inclination solutions. Using Eq. 35, the number of steps per revolution is 20,000.

$$Total\ Microsteps = \frac{360 * (Step\ Resolution)^{-1}}{Full\ Step\ Angle} \quad (35)$$

Equation 35. Microsteps

Regarding the inclination plane rotation, the most critical aspect is to ensure that, during the plane's stationary motion, the motor remains stationary. For that, Eq. 36 would be used to calculate the holding torque.

$$\tau = m * g * d \quad (36)$$

Equation 36. Torque

Where:

τ = torque

m = mass

d = perpendicular distance from the pivot

The mass acting during the motor's rotation would be divided into two main components: the acrylic inclined plane and the bioreactor with its motor. The acrylic plane has a length of 0.127m, a width of 0.1524 m, a thickness of 0.00635m, and a density of $1190 \frac{kg}{m^3}$, the distance from the pivot point is 0.0635m. As for the bioreactor and motor, their total mass is the sum of 0.08kg and 0.28kg, with 0.0508m from the pivot. Additionally, to ensure safety, a safety factor of 2 would be used. For this, the holding torque is calculated to be 0.542 Nm. Since the camera component was not taken into consideration due to the unknown mass, the acceptable holding torque would be about 0.55-0.6 Nm.

The Nema 23 173.5 in-oz has a maximum holding torque of 1.225 Nm [102]. Since the holding torque exceeds the maximum opposing torque, the motor is suitable. The maximum temperature reaches 266 °F (130 °C), exceeding the incubator's temperature limit [102]. Additionally, the motor has a current rate per phase of 2.8A and has a step angle of 1.8° [102]. Since this component is a stepper motor, a stepper driver has been selected to enable more precise rotational movement. The digital stepper driver used has a current per phase of 2.35-8A [103]. Since the current per phase of the motor is within the driver's range, the driver would be applicable. It has a maximum temperature of 85 °C, exceeding the incubator's temperature [103]. Furthermore, the maximum step resolution is one hundredth, allowing the driver to divide a complete step into 100 smaller steps [103]. This enhances the variation in angle increments in the prototype, thereby enabling a broader range of inclination solutions.

The microcontroller employed for direct motor control is the Arduino GIGA R1 WiFi, which incorporates a dual-core that can be programmed separately [104]. A key feature of this Arduino is its capability to connect to Wi-Fi [104]. Additionally, it has Bluetooth connectivity capabilities [104]. Finally, since there are a lot of pins needed for this project, the Arduino comes with 76 GPIOs and several communication buses [104].

5.2 Base Material

Acrylic sheets must be utilized as the foundational material for the prototype [105]. Given that the prototype will be positioned within the incubator and tests are anticipated to be conducted therein, the incubator's humidity and temperature are likely to influence the base material of the prototype.

The physical properties of the acrylic sheets, as determined by the ASTM method D648, show that a thickness of 0.236mm has a deflection temperature under a load of 264 psi of 99 °C, and the forming temperature ranges from 170 to 190 °C [105]. The softening point, as determined by the ASTM method D1525, is 115 °C, with a maximum recommended continuous service temperature of 82 °C [105]. Since the incubator would have a temperature significantly lower than the temperatures stated above, the minimum width of the acrylic sheets would be 0.236mm.

Additionally, the acrylic exhibits good insulating properties, with a surface resistivity higher than that of most plastics, making it a viable protector of the electrical components in the prototype. Due to humidity exposure, the acrylic is expected to expand by 0.6%, 0.4%, and 0.2% at humidities of 100%, 80%, and 60%, respectively [105].

Additionally, we need to ensure that the prototype will not degrade in the presence of chemical additives. Another limitation is the use of isopropyl alcohol (the most used alcohol in labs). Acrylic has limited resistance to this chemical [105]. Therefore, it is advisable to avoid using alcohol on the surface or placing the prototype on a surface with alcohol to ensure longevity. However, since there is limited resistance, it will be stated that limiting the use of alcohol is a must.

5.3 Rod

To achieve the inclination angles, the plane must undergo rotation. This rotation is facilitated by connecting the inclined plane to a rod that transfers linear motion into rotational motion. The choice of material for the rod is critical to the prototype's viability and safety. Accordingly, aluminum is selected as the material for the rod.

A primary characteristic of aluminum is its combination of lightness and strength [106]. Given that the inclined plane, in conjunction with the NEMA 17 and the bioreactor, contributes to the overall weight the rod must support, aluminum is the most suitable material. As the rod will be supported at its end, it is advantageous that the material's weight does not augment the stresses at these points.

Additionally, aluminum has a melting point of 660°C, which is higher than the incubator temperature, ensuring its stability [106]. Regarding the incubator, aluminum is non-corrosive due to its protective oxide layer; however, it can corrode if exposed to highly alkaline or acidic environments for extended periods [106]. Therefore, it is advisable to be cautious and avoid direct contact between aluminum and acidic or alkaline chemicals [119]. As a safety feature, aluminum is ductile and malleable [106]. In the event of failure, aluminum absorbs significant energy before breaking and deforms before failure [106]. This property provides a visual warning that the prototype may fail before it does.

5.4 Bioreactor

For the bioreactor, the part was recreated to accommodate the new materials available on the market. Using the provided CAD, the layers could be generated [64]. The structural layers of the bioreactor are as follows: top plate, bubble plate, gasket, spatial area, gas membrane, and bottom plate [64]. Since each layer

is separated, all the layers have cut-out holes around their circumference. The layers are then stacked and bolted together, as shown in Figure 20.

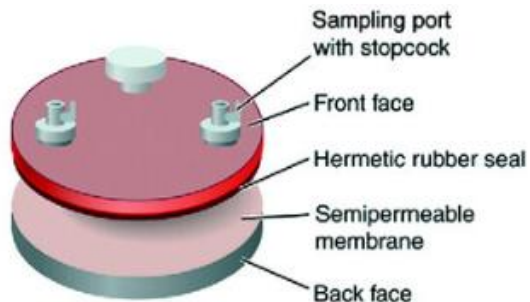


Figure 20: HARV Layers

6. Prototype

6.1 Wiring

After discussing the components of the prototype, various electrical components will require connections. Initially, it is essential to possess two motors and two stepper motor drivers. The rationale for this requirement is that one motor will be connected to the bioreactor to facilitate its rotation, and the other motor will be attached to the rod that rotates the plane. Considering that the motors used have high torque, it is impractical to connect both to a single driver. Connecting them to a single driver would result in current division between the two motors. Since these motors demand more than three-fourths of the available current, such a setup would increase hazards and compromise system safety. Although procuring two drivers incurs higher costs, electrical safety remains a primary design consideration. Additionally, this would allow the wiring to be neat and aligned with the prototype's needs.

The motors have four wires, which should be connected to the corresponding terminals on the stepper motor driver: A-, A+, B-, and B+. The stepper driver is interfaced with the Arduino via the following connections: STEPS+, DIRECTION+, ENABLE+, and GND. The STEP+ connection controls the number of steps, thereby controlling the shaft's rotation. The DIRECTION+ connection determines the rotation direction. The ENABLE+ connection specifies whether the rotational system will be operated manually or exclusively by the driver.

The negatives of STEP, DIRECTION, and ENABLE shall be connected to GND. While this is not obligatory, ensuring they remain disabled would enhance safety. Regarding GND, the entire system must be referenced to a common ground to ensure safety and comply with wiring standards.

Given that emergency safety is a critical requirement for the prototype, activating the stop button must halt all system motion. Accordingly, the VCD of the drivers is linked to one terminal of the stop button, while the opposite terminal is connected to the power source (power plug). The Arduino is powered independently via a battery, ensuring a dedicated power supply. Nevertheless, the battery grounds the Arduino, which is also connected to the drivers' GND, thereby ensuring uniform grounding across all components. Using KiCad, [Figure 21](#) illustrates the electrical connections displayed in the schematic.

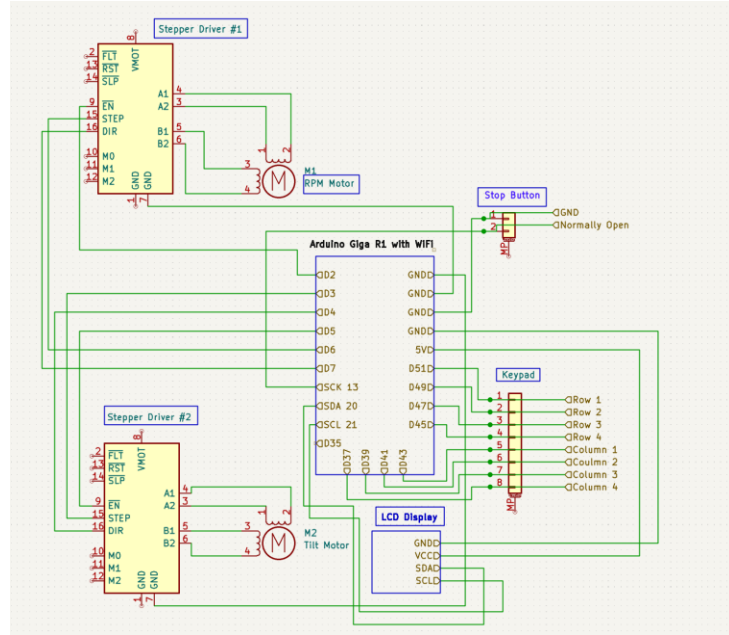


Figure 21: Electrical Schematic

6.2 Overall Prototype Basics

With the components assembled and the electrical connections established, the prototype could then be constructed.

Constrained by the dimensions of the incubator, the prototype should not exceed the specified limits of the incubator: $23 \times 17 \times 14$ in. As Figure 22 illustrates, the dimensions of the initial prototype estimate are significantly smaller than these constraints, with a value of $11.9 \times 13.0 \times 2.95$ in. The dimensions could be reduced by cutting off the excess portion of the rod; even at this size, it still fits the incubator.

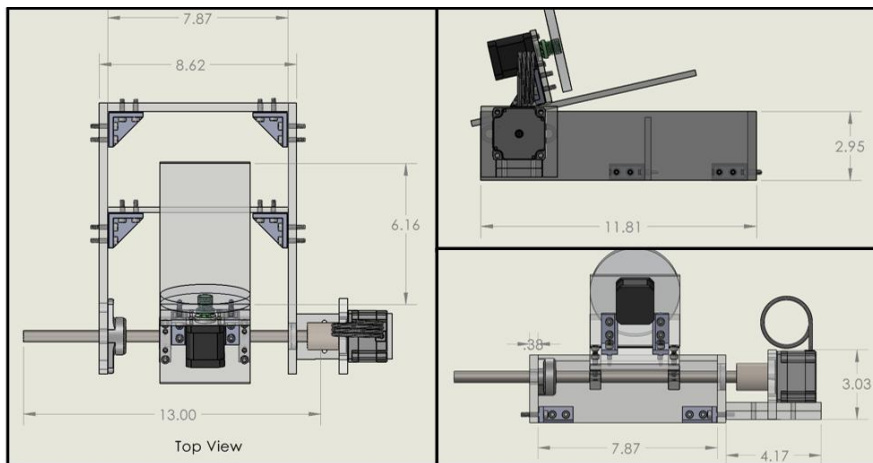


Figure 22. Prototype Dimensions (inches)

The prototype initially comprises a rectangular acrylic sheet base. An aluminum rod is positioned along two parallel sides of the base. The aluminum rod allows the inclined plane to rotate, as its movement requires a specific angle. The most straightforward and effective way to automatically facilitate this rotation is to use a rotatable rod.

To enable the rotation of the rod, it must be connected to a suitable motor capable of facilitating such motion. Accordingly, the rod is affixed to the NEMA 23 stepper motor. Since the rod's diameter is 0.5 in, it is connected to the motor shaft via a coupler. Nevertheless, it is imperative to secure the aluminum rod in position. To achieve this, bearings are installed at both ends of the rod.

A ball bearing is positioned at the end nearest the motor to facilitate smooth rotation and prevent increased stress on the motor shaft. The rod is subsequently connected to the inclined plane via two aluminum brackets. These brackets fit snugly into the rod through their circular holes and are fastened to the inclined plane at the horizontal section. The horizontal section attached to the inclined plane supports the bioreactor and the motor. The bioreactor is coupled to the motor using the motor coupler. The motor is secured in place by being screwed to the horizontal section.

The base is secured using L-shaped brackets to ensure stability. Furthermore, the inclined plane and the bioreactor plane are also supported by L-shaped brackets. The additional components in the prototype include a modification to the thickness of the front width of the base to ensure that the inclined plane does not topple from the initial angle. The detachable camera is positioned at the end of the inclined plane, seen in [Figure 23](#). A safety wall is installed to prevent the inclined plane from exceeding 0 or 90 degrees, as seen in [Figure 24](#). A box is made to ensure the electrical wiring, keypad, and emergency button are connected.

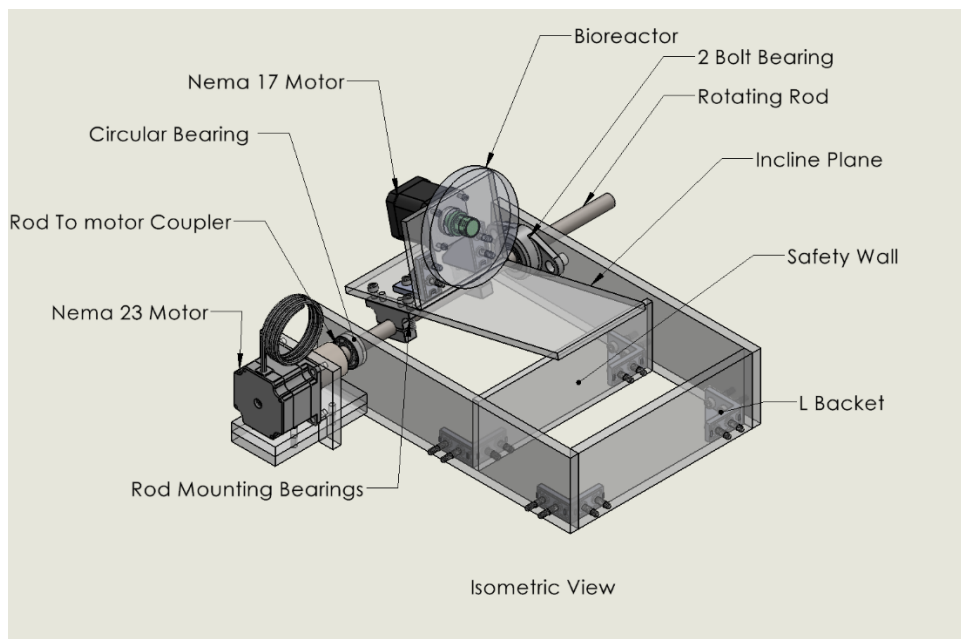


Figure 23. Isometric View of Prototype CAD

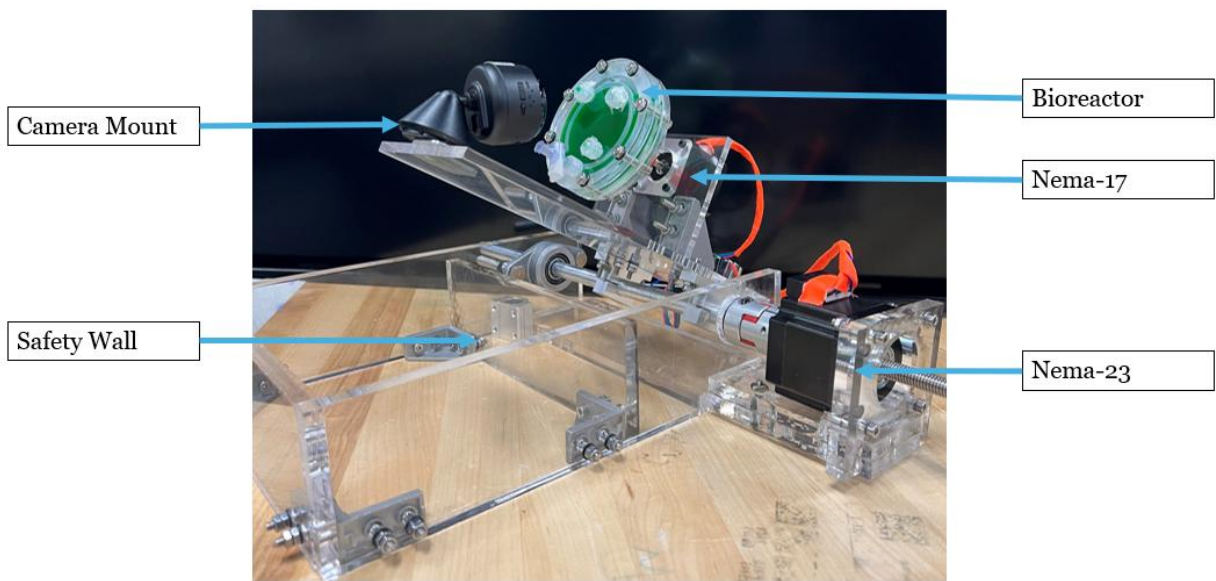


Figure 24: Prototype Angled View

7. Test Methods

To guarantee the validity of the results and decisions, specific tests must be conducted.

To validate the prototype, specific tests were conducted to quantify the effects of simulated gravity on the specimen. Since gravity is only tested by its impact on a mass, there are two ways in which gravity's effect is induced on the specimen in this prototype: RPM and inclination angle. Accordingly, the RPM Validation Test and the Inclination Angle Test were performed to assess these components.

The platform's tilt is a critical element in simulating partial gravity. The Inclination Angle Test was conducted to assess the accuracy of the tilt relative to the programmed angles. Images of the prototype were captured at eye level using a phone, with the platform tilted in 10° increments from 0° to 90°. Three images were taken at each step to assess stability. The angles in the image were measured three times in ImageJ to ensure accuracy. Statistical analysis, including the calculation of means and standard deviations, was performed in R. Finally, a linearity test was conducted to compare the measured angles with the expected angles.

To minimize shear on the specimen, the platform's rotational speed must remain constant. The RPM Validation Test was conducted to evaluate two criteria: the prototype's ability to generate the intended gravitational effect and to maintain steady flow under partial gravity. A tachometer was used to measure rotational speeds ranging from 5 RPM to 60 RPM in 5 RPM increments. For each RPM setting, three measurements were recorded at 30-second intervals to evaluate stability over time. Statistical analysis, including mean and standard deviation calculations, was performed in R for each RPM condition. Finally, the linearity between the measured and target RPMs was assessed to verify the accuracy of the rotational control.

The Alginate Bead Flow Test was conducted to verify that the specimen follows a circulator trajectory under partial gravity and to provide visual confirmation of steady flow. Alginate beads, a type of natural polymer widely used in drug delivery and cell studies, were selected to "mimic" cells due to their controllable size and encapsulation properties [107]. The droplet size during formation determines the bead size, offering flexibility in producing "mimic cells" of varying dimensions. Beads were made using the extrusion dripping method [108]. Due to their dispersive properties, visualization was achieved using dark-field imaging. For the test, a replica of the Alginate Bead Fluid Dynamics Validation was run [64]. A one-minute video was recorded for each condition using a stabilized camera aligned parallel to the inclined plane. Videos were analyzed in MATLAB to extract particle motion and generate trajectory graphs.

To ensure cell viability in the bioreactor, all materials in contact with the cells must be biocompatible and free of cytotoxic compounds. Compliance with ISO 10993-5: Tests for In Vitro Cytotoxicity was maintained to verify that the materials did not induce cell deformation or lysis [109]. The Indirect Contact Test assessed cell viability resulting from material-medium interactions [110]. Although L929 cells are the standard for cytotoxicity evaluation, NIH/3T3 cells were used in this study due to material availability constraints [111].

For the Indirect Contact Test, NIH/3T3 cells were seeded in T25 flasks and cultured to approximately 70% confluence [110]. Cells were then plated in a 96-well plate at a density of 1.0×10^5 cells per mL, with 50 µL of DMEM/FBS medium added to each well, bringing the total volume to 100 µL [110]. Two material samples- Nylon 500 mesh and Tegaderm- were incubated for 24 hours with a surface area-to-media ratio of 3mm²/mL [112]. The medium in the wells was subsequently replaced with the material-conditioned medium. Each sample was tested in triplicate and analyzed in diluted (50%) concentrations. Negative controls consisted of cells cultured with standard DMEM/FBS, while positive controls received PEI treatment [110]. The plate was incubated for 24 hours, after which 10% v/v Presto-Blue reagent was added to the medium for 5–10 minutes. Fluorescence readings were used to quantify cell viability. Data analysis was performed in R, and normality and variance were assessed before a one-sided unpaired t-test ($\alpha = 0.01$), with the null hypothesis that cell viability in contact with each material would be equal to or greater than the normal cell viability.

8. Results

RPM and Tilt Validation Tests

Measurements across the targeted RPM settings showed that the system provides values identical to the programmed RPMs with minimal variability. For each target RPM, the percentage error of the technical replicates was less than 1.5%, indicating good repeatability of the measurement process, supported by the small error bars in [Figure 25A](#).

Running the *lm* function in R to find the linearity of the data, the equation was the following:

$$y = 0.99x - 0.06$$

With a slope of 0.99, there is a 0.81% error from the ideal slope. With that, it confirms that the measured and intended RPMs are the same, demonstrating the accuracy of the device and code for RPM. The R-squared value of the fit is 0.999, indicating that a linear fit is the most appropriate model. However, the intercept value of 0.06 is slightly higher than expected. With a percentage error of 6.4%, the difference could be due to experimental/ sampling errors.

As for the tilt angles, the system showed that the measured values match the programmed values. With little to no variability, the errors bars (which are barely seen in [Figure 25B](#)) show little variability.

Running the *lm* function in R to find the linearity of the data, the equation was the following:

$$y = 1.03x - 0.4$$

With a slope of 1.03, there is a 3% error from the ideal slope. With that, it confirms that the measured and intended tilts are the same, demonstrating the accuracy of the device and code for tilt. The R-squared value of the fit is 0.999, indicating that a linear fit is the most appropriate model. However, the y-intercept value of 0.4 is slightly higher than expected.

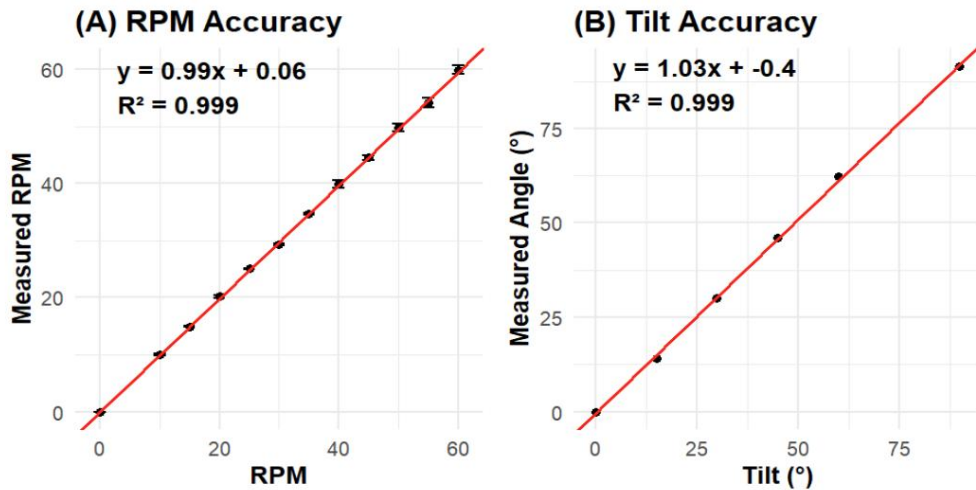


Figure 25. RPM and Tilt Validation

The figure shows the linear regression line. (A) The graph displays targeted RPM versus measured RPM. (B) The graph shows the targeted tilt versus the measured tilt.

Alginate Bead Test

For the alginate bead test, the goal is to observe a uniform circular flow. Using the recorded video and transferring it to MATLAB for analysis, the particle trajectories resemble those of the reference data (Dr. Phelan's alginate bead fluid validation test), as shown in [Figure 26](#) [64]. This confirmed a uniform circular trajectory.

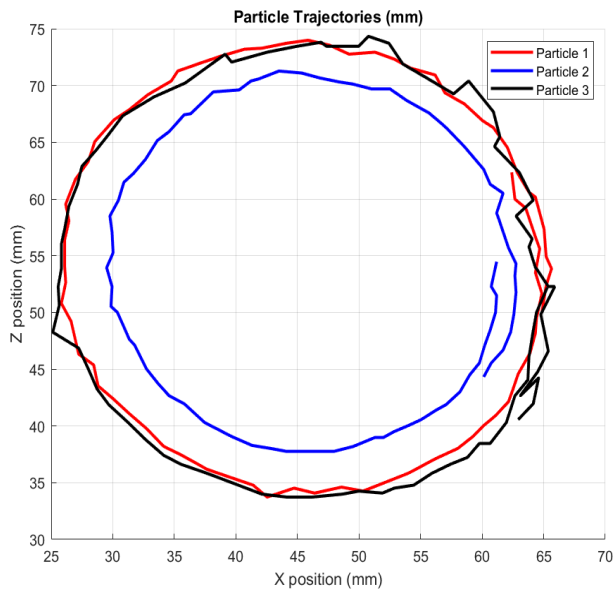


Figure 26. Alginate Bead Particle Motion

The figure shows the trajectory of the particles in one run of the bioreactor.

Indirect Contact Test

Cell viability was assessed for two materials: Nylon 500 mesh and Tegaderm. Individual replicates for each condition are shown in [Figure 27](#), with the mean value indicated below each group and the standard deviation represented.

For the Nylon 500 Mesh, the mean variability was 137.9%. Tegaderm had a mean viability of 95.1%. The results of the Levene Test (for variance) and the Shapiro-Wilk Test (for normality) indicated that all groups had normal distributions and equal variances.

Statistical analysis using a one-sided unpaired t-test revealed no significant differences in cell viability between the conditions and the healthy cell culture. Overall, all the materials exhibited high cell viability at a 50% dilution; Therefore, the null hypothesis has not been refuted, making the Tegaderm and Nylon 500 mesh acceptable material choices.

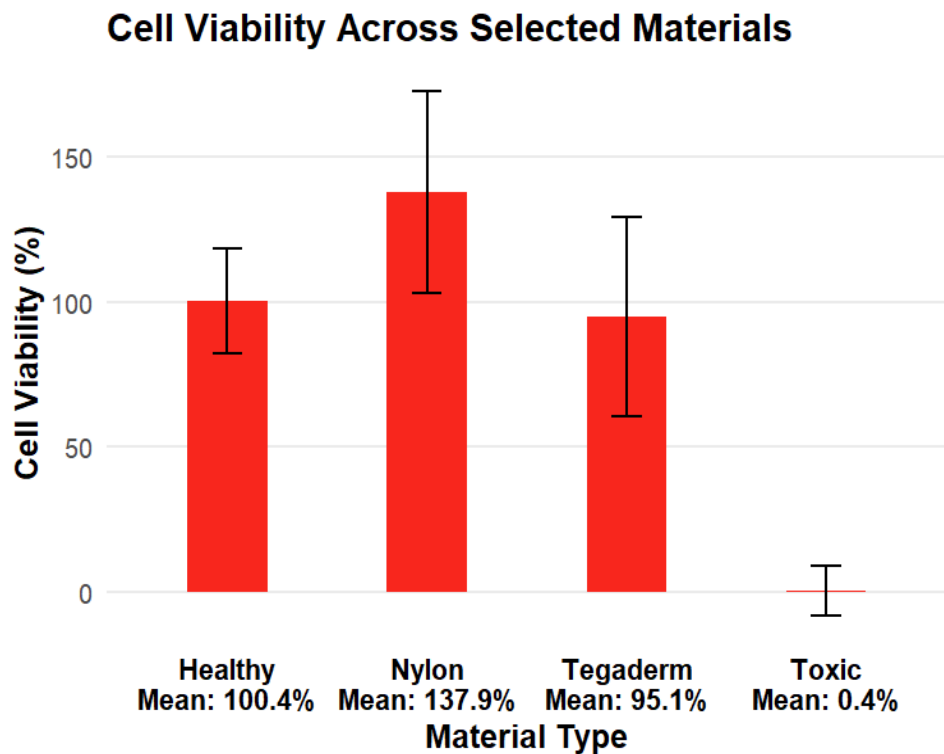


Figure 27. Cell Viability Per Material

The figure displays a scatter plot of cell viability across different conditions: healthy, toxic, nylon 500 mesh, and Tegaderm. The graph also shows the standard deviation for each group, along with its mean.

9. Cost

As for the cost, the prototype's per-unit cost would be roughly \$615.00. This price is a rough estimation based on over-pricing and lowering the prices of different materials. The materials listed in Table 6 were discussed in the Components and Prototype sections.

Table 6: Material Cost

Material	Price
Arduino Giga R1 Wi-Fi	\$48.72
Latching Emergency Stop Push Button Switch	\$11.99
IPS Weld-On 3 Acrylic Plastic Cement	\$26.99
Acrylic Sheet 3/8" Thick Cast	\$49.99
Nylon Mesh 300	\$15.99
3M Tegaderm Roll	\$25.81
Translucent Silicone Rubber 1/32" Thickness	\$11.99
½" Diameter Aluminum Rod	\$11.99
¼" Thick Clear Cast Acrylic	\$9.99
Sun-Founder Elite Explorer Kit	\$95.99
Luer Lock Tube Coupling ¼"-28	\$9.26
Nema 23 Stepper Motor + Stepper Driver	\$112.34
Nema 17 Stepper Motor + Stepper Driver	\$45.99
Aluminum Easy-Access Base-Mounted Shaft Support (1/2")	\$56.4
Mounted Ball Bearing	\$25.14
Ball Bearing	\$30.3
Motor Nema 23 to Shaft Coupler	\$9.19
Motor Nema 17 to Shaft Coupler	\$10.39

10. Summary and Conclusion

Overall, the prototype can simulate partial gravity using rotation and tilting. A created program enables a deeper understanding of particle and fluid properties, as well as gravity within the bioreactor. Looking at Table 7, all the criteria for the prototype were met except the computational model, which was a negotiable criterion. Therefore, it is reasonable to consider this prototype a success.

Table 7: Prototype Criteria

#	Priority	Requirement	Metric	Target Values/ Range or Pass/Fail	Justification	Met?
1	Non-negotiable	Gravitational Type	Partial Gravity and Controls	Range: μG to $1G$ Lunar gravity ($\frac{1}{6}G$) Martian gravity ($\frac{3}{8}G$) Earth's gravity (1G) Microgravity (μG)	NASA's Goals [50]	Yes
2	Non-negotiable	Uniform Trajectory	Partial Gravity Accuracy	Pass/ Fail Using Model and Visuals	Inaccuracy of data due to cell sensitivity [52]	Yes
3	Non-negotiable	Mathematical Simulation	Mathematical Model	Pass/ Fail	Accuracy and Validation	Yes
4	Non-negotiable	Overall Device Size	Dimensions	$23 \times 17 \times 14 \text{ in}$	Nuaire NU-5810E Incubator Restricted Area [54]	Yes
5	Non-negotiable	Electrical Safety	Safety	Pass/ Fail of EN61010-2-030	IEC 60204-1 [55, p. 60]	Yes
6	Non-negotiable	Emergency Safety	Safety	Pass/ Fail of ISO 13850	ISO 13850 [57]	Yes
7	Non-negotiable	Material	Strength, Durability, and Sterility	Pass/ Fail to withstand room temperature and 37°C, along with 98% humidity [54]	Safety	Yes

8	Negotiable	Cell Viability	Proper Cell Culture	>80%	ASTM F2739-19 [58]	Yes
9	Negotiable	Automated Imaging System	Data Tracking	> 30 FPS	To record the cell's activity during culturing	Yes
10	Negotiable	Computational Models	Modeling Accuracy	Pass/ Fail	To have a more sophisticated model for partial gravity	No

The main limitation was the inability to understand ANSYS within the given timeframe. Additionally, various enhancements are needed. First, the mathematical model should be more advanced. As of now, only viscosity and concentration are the main variables affecting shear and RPM; however, gas exchange and nutrient supply also significantly affect fluid properties. Second, the velocity gradient should be incorporated to determine the true required RPM, rather than simply testing whether a “guessed” RPM would suffice. Additionally, the prototype itself had issues, including imbalanced weights. There are two weights on the back of the plane to balance it out during tilting; however, rebuilding it would be more appropriate.

Since the project has a long way to go before it is finalized, a GitHub page was made. The account name is zozo2702, and the project name is Partial-Gravity-Bioreactor-Fa25. All the content and data used will be uploaded and made public to ensure anyone interested can learn more about the project.

11. References

- [1] “April 1961 - First Human Entered Space - NASA.” Accessed: Nov. 15, 2025. [Online]. Available: <https://www.nasa.gov/image-article/april-1961-first-human-entered-space/>
- [2] “Croatian Barrel Theory | Miro (Mike) Laus,” Mike Laus. Accessed: Nov. 15, 2025. [Online]. Available: <https://www.miromikelaus.com>
- [3] M. (Mike) Laus, Croatian Barrel Theory: Origin of the Solar System and Theory of First Cell on Earth. FriesenPress, 2025.
- [4] A. M. published, “10 Wild Theories About the Universe,” Live Science. Accessed: Nov. 15, 2025. [Online]. Available: <https://www.livescience.com/strange-theories-about-the-universe.html>
- [5] R. H. Sanders and S. S. McGaugh, “Modified Newtonian Dynamics as an Alternative to Dark Matter,” *Annu. Rev. Astron. Astrophys.*, vol. 40, no. Volume 40, 2002, p. 263–317, Sept. 2002, doi: 10.1146/annurev.astro.40.060401.093923.
- [6] B. Famaey and A. Durakovic, “Modified Newtonian Dynamics (MOND),” Jan. 28, 2025, arXiv: arXiv:2501.17006. doi: 10.48550/arXiv.2501.17006.
- [7] “Studying Combustion and Fire Safety - NASA.” Accessed: Nov. 15, 2025. [Online]. Available: <https://www.nasa.gov/missions/station/iss-research/studying-combustion-and-fire-safety/>
- [8] J. K. Gullari, “The Impact of Moon Phases on Earth, Plants, and Humans: A Comprehensive Study from Project Alpha,” Jan. 09, 2025, Social Science Research Network, Rochester, NY: 5090101. doi: 10.2139/ssrn.5090101.
- [9] J. Green, D. Draper, S. Boardsen, and C. Dong, “When the Moon Had a Magnetosphere,” *Sci. Adv.*, vol. 6, no. 42, p. eabc0865, Oct. 2020, doi: 10.1126/sciadv.abc0865.
- [10] “Mars Exploration - NASA Science.” Accessed: Nov. 15, 2025. [Online]. Available: <https://science.nasa.gov/planetary-science/programs/mars-exploration/>
- [11] “Why Go to Mars?” Accessed: Nov. 15, 2025. [Online]. Available: https://www.esa.int/Science_Exploration/Human_and_Robotic_Exploration/Exploration/Why_go_to_Mars
- [12] “The Combined Effects of Artificial Gravity, Temperature, and Hypoxia on Haemodynamic Responses and Limb Blood Flow | European Journal of Applied Physiology.” Accessed: Nov. 15, 2025. [Online]. Available: <https://link.springer.com/article/10.1007/s00421-025-05773-7>
- [13] S. A. Narayanan, “Gravity’s Effect on Biology,” *Front. Physiol.*, vol. 14, p. 1199175, July 2023, doi: 10.3389/fphys.2023.1199175.
- [14] “The Impact of Gravity on Life,” in *Evolution on Planet Earth*, Academic Press, 2003, p. 143–159. doi: 10.1016/B978-012598655-7/50036-7.
- [15] N. E. Ward, N. R. Pellis, S. A. Risin, and D. Risin, “Gene Expression Alterations in Activated Human T-Cells Induced By Modeled Microgravity,” *J. Cell. Biochem.*, vol. 99, no. 4, p. 1187–1202, Nov. 2006, doi: 10.1002/jcb.20988.
- [16] M. L. Lewis et al., “cDNA Microarray Reveals Altered Cytoskeletal Gene Expression in Space-Flown Leukemic T Lymphocytes (Jurkat),” *FASEB J. Off. Publ. Fed. Am. Soc. Exp. Biol.*, vol. 15, no. 10, p. 1783–1785, Aug. 2001, doi: 10.1096/fj.00-0820fje.
- [17] S. Tauber, S. Christoffel, C. S. Thiel, and O. Ullrich, “Transcriptional Homeostasis of Oxidative Stress-Related Pathways in Altered Gravity,” *Int. J. Mol. Sci.*, vol. 19, no. 9, p. 2814, Sept. 2018, doi: 10.3390/ijms19092814.
- [18] T. T. Chang et al., “The Rel/NF-κB Pathway and Transcription of Immediate Early Genes in T Cell Activation Are Inhibited by Microgravity,” *J. Leukoc. Biol.*, vol. 92, no. 6, p. 1133–1145, Dec. 2012, doi: 10.1189/jlb.0312157.
- [19] E. S. Baker, M. R. Barratt, C. F. Sams, and M. L. Wear, “Human Response to Space Flight,” in *Principles of Clinical Medicine for Space Flight*, M. R. Barratt, E. S. Baker, and S. L. Pool, Eds., New York, NY: Springer, 2019, p. 367–411. doi: 10.1007/978-1-4939-9889-0_12.
- [20] A. D. Moore, M. E. Downs, S. M. C. Lee, A. H. Feiveson, P. Knudsen, and L. Ploutz-Snyder, “Peak Exercise Oxygen Uptake During and Following Long-Duration Spaceflight,” *APSselect*, vol. 1, no. 9, p. 231–238, Sept. 2014, doi: 10.1152/japplphysiol.01251.2013@apsselect.2014.1.issue-9.
- [21] “Exercise in Space: Human Skeletal Muscle After 6 Months Aboard the International Space Station | Journal of Applied Physiology | American Physiological Society.” Accessed: Nov. 15, 2025. [Online]. Available:

- <https://journals.physiology.org/doi/full/10.1152/japplphysiol.91578.2008?hits=10&HITS=10&author1=Trappe%2C+S&searchid=1&sortspe=&maxtoshow=&FIRSTINDEX=0&RESULTFORMAT=>
- [22] J. D. Sibonga, E. R. Spector, S. L. Johnston, and W. J. Tarver, “Evaluating Bone Loss in ISS Astronauts,” *Aerosp. Med. Hum. Perform.*, vol. 86, no. 12 Suppl, p. A38–A44, Dec. 2015, doi: 10.3357/AMHP.EC06.2015.
- [23] C. Richter, B. Braunstein, A. Winnard, M. Nasser, and T. Weber, “Human Biomechanical and Cardiopulmonary Responses to Partial Gravity – A Systematic Review,” *Front. Physiol.*, vol. 8, Aug. 2017, doi: 10.3389/fphys.2017.00583.
- [24] “Apollo 15: Mission Details - NASA.” Accessed: Nov. 15, 2025. [Online]. Available: <https://www.nasa.gov/missions/apollo/apollo-15-mission-details/>
- [25] Apollo11Space, “Apollo Program Costs (New Data 1969 vs 2024),” Apollo11Space. Accessed: Nov. 15, 2025. [Online]. Available: <https://apollo11space.com/apollo-program-costs-new-data-1969-vs-2024/>
- [26] Apollo11Space, “Apollo Program Failures and Lessons Learned: NASA’s Journey to the Moon,” Apollo11Space. Accessed: Nov. 15, 2025. [Online]. Available: <https://apollo11space.com/apollo-program-failures-and-lessons-learned-nasas-journey-to-the-moon/>
- [27] “Twins Study - NASA.” Accessed: Nov. 15, 2025. [Online]. Available: <https://www.nasa.gov/humans-in-space/twins-study/>
- [28] “The NASA Twins Study: A Multidimensional Analysis of A Year-Long Human Spaceflight | Science.” Accessed: Nov. 15, 2025. [Online]. Available: <https://www.science.org/doi/10.1126/science.aau8650>
- [29] S. Zhang, T. Adachi, S. Zhang, Y. Yoshida, and A. Takahashi, “A New Type of Simulated Partial Gravity Apparatus For Rats Based On A Pully-Spring System,” *Front. Cell Dev. Biol.*, vol. 10, p. 965656, Aug. 2022, doi: 10.3389/fcell.2022.965656.
- [30] J. Sánchez-Haro, I. Lombillo, and G. Capellán, “Simplified Model to Consider Influence of Gravity on Impacts on Structures: Experimental and Numerical Validation,” *Int. J. Impact Eng.*, vol. 173, p. 104474, Mar. 2023, doi: 10.1016/j.ijimpeng.2022.104474.
- [31] J. Wong, “Cells in Space,” *Nat. Med.*, vol. 3, no. 3, p. 259–259, Mar. 1997, doi: 10.1038/nm0397-259b.
- [32] “Gravity | Definition, Physics, & Facts | Britannica.” Accessed: Nov. 15, 2025. [Online]. Available: <https://www.britannica.com/science/gravity-physics>
- [33] “Physical Constant | Definition, Examples & Units | Britannica.” Accessed: Nov. 15, 2025. [Online]. Available: <https://www.britannica.com/science/physical-constant>
- [34] “Zero Gravity Noun - Definition, Pictures, Pronunciation and Usage Notes | Oxford Advanced Learner’s Dictionary at OxfordLearnersDictionaries.com.” Accessed: Nov. 15, 2025. [Online]. Available: <https://www.oxfordlearnersdictionaries.com/definition/english/zero-gravity>
- [35] “What is Microgravity? - NASA.” Accessed: Nov. 15, 2025. [Online]. Available: <https://www.nasa.gov/centers-and-facilities/glenn/what-is-microgravity/>
- [36] A. Manzano et al., “Novel, Moon and Mars, Partial Gravity Simulation Paradigms and Their Effects on the Balance Between Cell Growth and Cell Proliferation During Early plant development,” *Npj Microgravity*, vol. 4, no. 1, p. 9, Apr. 2018, doi: 10.1038/s41526-018-0041-4.
- [37] M. Stephenson and W. Grayson, “Recent Advances in Bioreactors for Cell-Based Therapies,” *F1000Research*, vol. 7, p. F1000 Faculty Rev-517, Apr. 2018, doi: 10.12688/f1000research.12533.1.
- [38] “NASA Bioreactors Advance Disease Treatments | NASA Spinoff.” Accessed: Nov. 15, 2025. [Online]. Available: https://spinoff.nasa.gov/Spinoff2009/hm_3.html
- [39] J. Loon, “Clinostats and Other Rotating Systems—Design, Function, and Limitations,” 2022, p. 147–156. doi: 10.1201/9781003338277-17.
- [40] T. Rs, “Chapter 8: Microbial Life in Space”.
- [41] V. Popova, T. Bilova, G. Smolikova, A. Frolov, and S. Medvedev, “3D-clinorotation Induces Specific Alterations in Metabolite Profiles of Germinating Brassica Napus L. Seeds,” *Biol. Commun.*, vol. 64, p. 55–74, Jan. 2019, doi: 10.21638/spbu03.2019.107.
- [42] F. J. Medina, A. Manzano, A. Villacampa, M. Ciska, and R. Herranz, “Understanding Reduced Gravity Effects on Early Plant Development Before Attempting Life-Support Farming in the Moon and Mars,” *Front. Astron. Space Sci.*, vol. 8, Sept. 2021, doi: 10.3389/fspas.2021.729154.
- [43] B. R. Unsworth and P. I. Lelkes, “Growing Tissues in Microgravity,” *Nat. Med.*, vol. 4, no. 8, p. 901–907, Aug. 1998, doi: 10.1038/nm0898-901.
- [44] “United Nations Sustainable Development Goals (SDGs),” United Nations Western Europe. Accessed: Nov. 15, 2025. [Online]. Available: <https://unric.org/en/united-nations-sustainable-development-goals/>
- [45] “Goal 3 | Department of Economic and Social Affairs.” Accessed: Nov. 15, 2025. [Online]. Available: <https://sdgs.un.org/goals/goal3>

- [46] “Goal 9 | Department of Economic and Social Affairs.” Accessed: Nov. 15, 2025. [Online]. Available: <https://sdgs.un.org/goals/goal9>
- [47] “Goal 12 | Department of Economic and Social Affairs.” Accessed: Nov. 16, 2025. [Online]. Available: <https://sdgs.un.org/goals/goal12>
- [48] F. Palladino et al., “Bioreactors: Applications and Innovations for a Sustainable and Healthy Future—A Critical Review,” *Appl. Sci.*, vol. 14, p. 9346, Oct. 2024, doi: 10.3390/app14209346.
- [49] “Goal 13 | Department of Economic and Social Affairs.” Accessed: Nov. 16, 2025. [Online]. Available: <https://sdgs.un.org/goals/goal13>
- [50] “Destinations - NASA.” Accessed: Nov. 16, 2025. [Online]. Available: <https://www.nasa.gov/humans-in-space/destinations/>
- [51] J. Swanenburg, C. A. Easthope, A. Meinke, A. Langenfeld, D. A. Green, and P. Schweinhardt, “Lunar and Mars Gravity Induce Similar Changes in Spinal Motor Control as Microgravity,” *Front. Physiol.*, vol. 14, p. 1196929, July 2023, doi: 10.3389/fphys.2023.1196929.
- [52] “Scientists Create Model to Measure How Cells Sense Their Surroundings,” ScienceDaily. Accessed: Nov. 16, 2025. [Online]. Available: <https://www.sciencedaily.com/releases/2020/03/200326144348.htm>
- [53] “Gravity: It’s Only a Theory | National Center for Science Education.” Accessed: Nov. 16, 2025. [Online]. Available: <https://ncse.ngo/gravity-its-only-theory>
- [54] “NU-5810 High Heat Decontamination CO₂ Incubator,” www.nuaire.com. Accessed: Nov. 16, 2025. [Online]. Available: <https://www.nuaire.com/products/co2-incubators/direct-heat/in-vitrocell-nu-5810-direct-heat-decon-co2-incubator>
- [55] Admin, “IEC 60204-1: Safety of Machinery and Electrical Equipment Design : Electrical Engineering Hub.” Accessed: Nov. 16, 2025. [Online]. Available: <https://azadtechhub.com/iec-60204-1-safety-of-machinery-and-electrical-equipment-design/>
- [56] “IEC 61010-2-030:2023.” Accessed: Nov. 16, 2025. [Online]. Available: <https://webstore.iec.ch/en/publication/75915>
- [57] “ISO 13850:2015,” ISO. Accessed: Nov. 16, 2025. [Online]. Available: <https://www.iso.org/standard/59970.html>
- [58] “Cell Culture: Growing Cells as Model Systems In Vitro,” in *Basic Science Methods for Clinical Researchers*, Academic Press, 2017, p. 151–172. doi: 10.1016/B978-0-12-803077-6.00009-6.
- [59] A. Simonyan and N. Sarvazyan, “Bioreactors,” in *Tissue Engineering: Principles, Protocols, and Practical Exercises*, N. Sarvazyan, Ed., Cham: Springer International Publishing, 2020, p. 127–136. doi: 10.1007/978-3-030-39698-5_11.
- [60] F. J. Armistead, J. G. D. Pablo, H. Gadêlha, S. A. Peyman, and S. D. Evans, “Cells Under Stress: An Inertial-Shear Microfluidic Determination of Cell Behavior,” *Biophys. J.*, vol. 116, no. 6, p. 1127–1135, Mar. 2019, doi: 10.1016/j.bpj.2019.01.034.
- [61] C. A. Nickerson, C. M. Ott, J. W. Wilson, R. Ramamurthy, and D. L. Pierson, “Microbial Responses to Microgravity and Other Low-Shear Environments,” *Microbiol. Mol. Biol. Rev.*, vol. 68, no. 2, pp. 345–361, June 2004, doi: 10.1128/MMBR.68.2.345-361.2004.
- [62] D. Nowacki, F. Klinger, G. Mazur, and M. De Felici, “Effect of Culture in Simulated Microgravity on the Development of Mouse Embryonic Testes,” *Adv. Clin. Exp. Med.*, vol. 24, pp. 769–774, Sept. 2015, doi: 10.17219/acem/27920.
- [63] H. Andrade, L. Santos, and A. León-Rodríguez, “Expansion of Human Hematopoietic Stem Cells for Transplantation: Trends And Perspectives,” *Cytotechnology*, vol. 56, pp. 151–60, Apr. 2008, doi: 10.1007/s10616-008-9144-1.
- [64] M. A. Phelan, A. L. Gianforcaro, J. A. Gerstenhaber, and P. I. Lelkes, “An Air Bubble-Isolating Rotating Wall Vessel Bioreactor for Improved Spheroid/Organoid Formation,” *Tissue Eng. Part C Methods*, vol. 25, no. 8, pp. 479–488, Aug. 2019, doi: 10.1089/ten.tec.2019.0088.
- [65] P. R. Cavanagh et al., “A Novel Lunar Bed Rest Analogue,” *Aviat. Space Environ. Med.*, vol. 84, no. 11, p. 1191–1195, Nov. 2013, doi: 10.3357/asem.3472.2013.
- [66] “VGM – A Novel Centrifuge For Partial Gravity Experiments and Cell Seeding in Microgravity — IAF Digital Library.”
- [67] G. Clément, A. Buckley, and W. Paloski, “Artificial Gravity as a Countermeasure for Mitigating Physiological Deconditioning During Long-Duration Space Missions,” *Front. Syst. Neurosci.*, vol. 9, p. 92, June 2015, doi: 10.3389/fnsys.2015.00092.
- [68] “Centripetal Acceleration | Physics.” Accessed: Dec. 07, 2025. [Online]. Available: <https://courses.lumenlearning.com/suny-physics/chapter/6-2-centripetal-acceleration/>

- [69] G. Clément, “International Roadmap for Artificial Gravity Research,” *Npj Microgravity*, vol. 3, no. 1, p. 29, Nov. 2017, doi: 10.1038/s41526-017-0034-8.
- [70] J.-L. Pérez-Pavón, S. Herrero-Martín, C. Pinto, and B. Cordero, “Determination of Trihalomethanes in Water Samples: A review,” *Anal. Chim. Acta*, vol. 629, p. 6–23, Dec. 2008, doi: 10.1016/j.aca.2008.09.042.
- [71] “Design and Performance of Single-Use, Stirred-Tank Bioreactors,” BioProcess International. Accessed: Dec. 07, 2025. [Online]. Available: <https://www.bioprocessintl.com/single-use/design-and-performance-of-single-use-stirred-tank-bioreactors>
- [72] “Weighted Decision Matrix: A Tool for Pro-Level Prioritization,” airfocus. Accessed: Dec. 07, 2025. [Online]. Available: <https://airfocus.com/blog/weighted-decision-matrix-prioritization/>
- [73] “Microgravity | Space Exploration, Astronauts & Zero-Gravity | Britannica.” Accessed: Dec. 07, 2025. [Online]. Available: <https://www.britannica.com/science/microgravity>
- [74] “Novel, Moon and Mars, Partial Gravity Simulation Paradigms and Their Effects on the Balance Between Cell Growth and Cell Proliferation During Early Plant Development | *npj Microgravity*.” Accessed: Dec. 07, 2025. [Online]. Available: <https://www.nature.com/articles/s41526-018-0041-4>
- [75] “Parabolic Flight - NASA.” Accessed: Dec. 07, 2025. [Online]. Available: <https://www.nasa.gov/mission/parabolic-flight/>
- [76] “Equivalence Principle | Gravitational, Acceleration & Time Dilation | Britannica.” Accessed: Dec. 07, 2025. [Online]. Available: <https://www.britannica.com/science/equivalence-principle>
- [77] V. Loon and J. J. W. A, “Centrifuges for Microgravity Simulation. The Reduced Gravity Paradigm,” *Front. Astron. Space Sci.*, vol. 3, July 2016, doi: 10.3389/fspas.2016.00021.
- [78] A. Barzegari and A. A. Saei, “An Update to Space Biomedical Research: Tissue Engineering in Microgravity Bioreactors,” *BioImpacts BI*, vol. 2, no. 1, p. 23–32, 2012, doi: 10.5681/bi.2012.003.
- [79] A. L. Radtke and M. M. Herbst-Kralovetz, “Culturing and Applications of Rotating Wall Vessel Bioreactor Derived 3D Epithelial Cell Models,” *J. Vis. Exp. JoVE*, no. 62, p. 3868, Apr. 2012, doi: 10.3791/3868.
- [80] P. M. Gershovich, J. G. Gershovich, A. P. Zhambalova, Yu. A. Romanov, and L. B. Buravkova, “Cytoskeletal Proteins and Stem Cell Markers Gene Expression in Human Bone Marrow Mesenchymal Stromal Cells After Different Periods of Simulated Microgravity,” *Acta Astronaut.*, vol. 70, p. 36–42, Jan. 2012, doi: 10.1016/j.actaastro.2011.07.028.
- [81] S. Navran, “The Application of Low Shear Modeled Microgravity to 3-D Cell Biology and Tissue Engineering,” *Biotechnol. Annu. Rev.*, vol. 14, p. 275–296, 2008, doi: 10.1016/S1387-2656(08)00011-2.
- [82] A. Wnorowski et al., “Effects of Spaceflight on Human Induced Pluripotent Stem Cell-Derived Cardiomyocyte Structure and Function,” *Stem Cell Rep.*, vol. 13, no. 6, p. 960–969, Dec. 2019, doi: 10.1016/j.stemcr.2019.10.006.
- [83] “(PDF) Microbial Monitoring of Crewed Habitats in Space—Current Status and Future Perspectives,” ResearchGate, Aug. 2025, doi: 10.1264/jsme2.ME14031.
- [84] “(PDF) Mars Artificial Gravity Habitat with Centrifugation (MAGICIAN),” in ResearchGate, doi: 10.1109/AERO58975.2024.10521126.
- [85] “Trigonometry | Definition, Formulas, Ratios, & Identities | Britannica.” Accessed: Dec. 07, 2025. [Online]. Available: <https://www.britannica.com/science/trigonometry>
- [86] TrueGeometry, “How to Calculate RPM from Angular Velocity In Context of RPM to Angular Velocity,” True Geometry’s Blog. Accessed: Dec. 07, 2025. [Online]. Available: https://blog.truegeometry.com/tutorials/education/b372e069150d103d6263046cc3742829/JSON_TO_ARTCL_How_to_Calculate_RPM_from_Angular_Velocity_in_context_of_rpm_to_an.html
- [87] “Settling Velocity - An Overview | ScienceDirect Topics.” Accessed: Dec. 07, 2025. [Online]. Available: <https://www.sciencedirect.com/topics/physics-and-astronomy/settling-velocity>
- [88] “Stokes’s law | Definition, Formula, & Facts | Britannica.” Accessed: Dec. 07, 2025. [Online]. Available: <https://www.britannica.com/science/Stokess-law>
- [89] “Reynolds’ Number - An Overview | ScienceDirect Topics.” Accessed: Dec. 07, 2025. [Online]. Available: <https://www.sciencedirect.com/topics/engineering/reynolds-number>
- [90] W. Zhu and H. Obara, “Flow Structure of Okra Mucilage in Rotating Wall Vessel System,” *Heliyon*, vol. 10, no. 16, p. e36149, Aug. 2024, doi: 10.1016/j.heliyon.2024.e36149.
- [91] J. A. Espina, M. H. Cordeiro, M. Milivojevic, I. Pajić-Lijaković, and E. H. Barriga, “Response of Cells and Tissues to Shear Stress,” *J. Cell Sci.*, vol. 136, no. 18, p. jcs260985, Sept. 2023, doi: 10.1242/jcs.260985.
- [92] “Fluid Shear Stress - An Overview | ScienceDirect Topics.” Accessed: Dec. 07, 2025. [Online]. Available: <https://www.sciencedirect.com/topics/engineering/fluid-shear-stress>

- [93] “Shear Stress - An Overview | ScienceDirect Topics.” Accessed: Dec. 07, 2025. [Online]. Available: <https://www.sciencedirect.com/topics/biochemistry-genetics-and-molecular-biology/shear-stress>
- [94] M. Mohsin, A. A. Zaidi, and B. van Brunt, “Dynamics of Cell Growth: Exponential Growth and Division After A Minimum Cell Size,” *Partial Differ. Equ. Appl. Math.*, vol. 11, p. 100814, Sept. 2024, doi: 10.1016/j.padiff.2024.100814.
- [95] “The Influence of Particles on Suspension Rheology | Anton Paar Wiki,” Anton Paar. Accessed: Dec. 07, 2025. [Online]. Available: <https://wiki.anton-paar.com/en/the-influence-of-particles-on-suspension-rheology/>
- [96] D. A. Charlebois and G. Balázs, “Modeling Cell Population Dynamics,” *In Silico Biol.*, vol. 13, no. 1–2, p. 21–39, doi: 10.3233/ISB-180470.
- [97] “Torque Formula (Moment of Inertia and Angular Acceleration).” Accessed: Dec. 07, 2025. [Online]. Available: https://www.softschools.com/formulas/physics/torque_formula/59/
- [98] “10.6: Calculating Moments of Inertia,” Physics LibreTexts. Accessed: Dec. 07, 2025. [Online]. Available: [https://phys.libretexts.org/Bookshelves/University_Physics/University_Physics_\(OpenStax\)/Book%3A_University_Physics_I_-_Mechanics_Sound_Oscillations_and_Waves_\(OpenStax\)/10%3A_Fixed-Axis_Rotation__Introduction/10.06%3A_Calculating_Moments_of_Inertia](https://phys.libretexts.org/Bookshelves/University_Physics/University_Physics_(OpenStax)/Book%3A_University_Physics_I_-_Mechanics_Sound_Oscillations_and_Waves_(OpenStax)/10%3A_Fixed-Axis_Rotation__Introduction/10.06%3A_Calculating_Moments_of_Inertia)
- [99] “Density Formula - How to Calculate Density.” Accessed: Dec. 07, 2025. [Online]. Available: <https://www.thecalculatorsite.com/articles/math/density-formula.php>
- [100] “Nema 17 Bipolar 1.8deg 65Ncm(92oz.in) 2.1A 42x42x60mm 4 Wires - 17HS24-2104S | StepperOnline.” Accessed: Dec. 07, 2025. [Online]. Available: <https://www.omc-stepperonline.com/nema-17-bipolar-1-8deg-65ncm-92oz-in-2-1a-3-36v-42x42x60mm-4-wires-17hs24-2104s>
- [101] “McMaster-Carr.” Accessed: Dec. 07, 2025. [Online]. Available: <https://www.mcmaster.com/>
- [102] “McMaster-Carr.” Accessed: Dec. 08, 2025. [Online]. Available: <https://www.mcmaster.com/>
- [103] “McMaster-Carr.” Accessed: Dec. 08, 2025. [Online]. Available: <https://www.mcmaster.com/>
- [104] “GIGA R1 WiFi | Arduino Documentation.” Accessed: Dec. 08, 2025. [Online]. Available: <https://docs.arduino.cc/hardware/giga-r1-wifi/>
- [105] “Physical Properties Acrylic | PDF.” Accessed: Dec. 08, 2025. [Online]. Available: <https://www.scribd.com/doc/143885302/Physical-Properties-Acrylic>
- [106] “Aluminum: Properties, Uses, and Benefits.” Accessed: Dec. 08, 2025. [Online]. Available: <https://www.thomasnet.com/articles/metals-metal-products/aluminum/>
- [107] D. M. Hariyadi and N. Islam, “Current Status of Alginate in Drug Delivery,” *Adv. Pharmacol. Pharm. Sci.*, vol. 2020, p. 8886095, 2020, doi: 10.1155/2020/8886095.
- [108] F. Davarci, D. Turan, B. Ozcelik, and D. Poncelet, “The Influence of Solution Viscosities and Surface Tension on Calcium-Alginate Microbead Formation Using Dripping Technique,” *Food Hydrocoll.*, vol. 62, p. 119–127, Jan. 2017, doi: 10.1016/j.foodhyd.2016.06.029.
- [109] “ISO 10993-5:2009,” ISO. Accessed: Dec. 08, 2025. [Online]. Available: <https://www.iso.org/standard/36406.html>
- [110] G. K. Srivastava et al., “Comparison Between Direct Contact and Extract Exposure Methods For PFO Cytotoxicity Evaluation,” *Sci. Rep.*, vol. 8, no. 1, p. 1425, Jan. 2018, doi: 10.1038/s41598-018-19428-5.
- [111] “NIH/3T3 (Atcc CRL 1658) : Product Sheet | PDF | Atcc (Company) | Cell Culture,” Scribd. Accessed: Dec. 08, 2025. [Online]. Available: <https://www.scribd.com/document/435514441/NIH-3T3>
- [112] S. Gruber, “Cytotoxicity Testing & ISO 10993-5: 7 Tips For Laboratory Selection,” Regulatory knowledge for medical devices. Accessed: Dec. 08, 2025. [Online]. Available: <https://blog.johner-institute.com/regulatory-affairs/cytotoxicity-testing/>

12. Supplementary Data

Supplementary Table S 1: Bioreactor Systems for Cell Expansion

Bioreactor type	Commercial examples	Parameter ranges	Advantages/limitations	Example case studies	References
Rocking bed (wave motion)	<ul style="list-style-type: none"> • WAVE (GE Healthcare) • Finesse (Thermo Fisher) • Biostat (Sartorius) 	<ul style="list-style-type: none"> • Size (1–500 L) • Rocking angle: 5–35° • Rotation speed: 10–35 rpm 	<p>Advantages:</p> <ul style="list-style-type: none"> • Versatile single-use bags <p>Limitations:</p> <ul style="list-style-type: none"> • Limited scale-up potential 	<ul style="list-style-type: none"> • Cell type: hMSCs • Method: microcarrier culture • Culture time: 7 days • Fold expansion: 0.7–14.5 • Metrics: viability, tri-lineage differentiation, aggregate size 	[1]
Stirred tank	<ul style="list-style-type: none"> • Mobius (EMD Millipore) • Finesse (Thermo Fisher) 	<ul style="list-style-type: none"> • Size (100 mL–1,000 L) • Impeller power/speed: variable during culture period • Impeller design: updraft or downdraft, single or multiple 	<p>Advantages:</p> <ul style="list-style-type: none"> • Functional at-large volumes: >50 L <p>Limitations:</p> <ul style="list-style-type: none"> • Shear forces may impact cell viability/differentiation 	<ul style="list-style-type: none"> • Cell type: hMSCs, hASCs, hiPSCs, and murine ovary cell cells • Method: aggregates, microcarriers, and single-cell suspensions • Culture time: 11–17 days • Fold expansion: 25.7–43 • Metrics: viability, aggregate size, and differentiation capacity 	[3][4][5][6]
Rotating wall vessels	RCCMAX (Synthecon)	<ul style="list-style-type: none"> • Size (100 mL–10 L) • Rotational speed: 5–20 rpm • Continuous medium recirculation or 	<p>Advantages:</p> <ul style="list-style-type: none"> • Low turbulence • Can simulate microgravity <p>Limitations:</p> <ul style="list-style-type: none"> • Effective only at small volumes: <10 L 	<ul style="list-style-type: none"> • Cell type: hMSCs • Method: scaffolds • Culture time: 21 days • Fold expansion: ~39 	[7]

Bioreactor type	Commercial examples	Parameter ranges	Advantages/limitations	Example case studies	References
		closed batch system		<ul style="list-style-type: none"> Metrics: viability, surface marker expression, and differentiation 	
Perfusion bioreactor	<ul style="list-style-type: none"> FiberCell (FiberCell Systems) Quantum Cell Expansion (Terumo BCT) 	<ul style="list-style-type: none"> Size (100 mL–5 L) Perfusion: direct (for example, through scaffolds) or indirect (hollow-fiber, encapsulated cells) 	<p>Advantages:</p> <ul style="list-style-type: none"> Limited turbulence Can be automated Compact <p>Limitations:</p> <ul style="list-style-type: none"> Shear forces may impact cell viability/differentiation 	<ul style="list-style-type: none"> Cell type: hMSCs Method: encapsulation Culture time: 21 days Fold expansion: not applicable Metrics: viability and differentiation 	[8][9]
Isolation/expansion automated systems	<ul style="list-style-type: none"> G-Rex (Wilson Wolf) CliniMACs Prodigy (Miltenyi Biotec) 	<ul style="list-style-type: none"> Size (100 mL) Degree of automation 	<p>Advantages:</p> <ul style="list-style-type: none"> Versatile single-use bags Automated cell isolation, manipulation, and expansion GMP-compliant <p>Limitations:</p> <ul style="list-style-type: none"> Primarily T-cell expansion 	<ul style="list-style-type: none"> Cell type: human lymphocytes Method: suspension culture Culture time: 8–14 days Fold expansion: 32–63 Metrics: viability and cell marker evaluation 	[10][11]

GMP, good manufacturing practices; hASC, human adipose-derived stem cell; hiPSC, human induced pluripotent stem cell; hMSC, human mesenchymal stem cell.

[Supplementary Table S 1](#) shows a summary of the different types of bioreactors for cell expansion. It includes their commercial examples, parameter ranges, advantages/ limitations, and example case studies [2].

13. Supplementary Data References

- 1) A. Shekaran et al., "Biodegradable ECM-coated PCL Microcarriers Support Scalable Human Early MSC Expansion and In Vivo Bone Formation," *Cytotherapy*, vol. 18, no. 10, p. 1332–1344, Aug. 2016, doi: 10.1016/j.jcyt.2016.06.016. Available: <https://pubmed.ncbi.nlm.nih.gov/27503763/>
- 2) M. Stephenson and W. Grayson, "Recent Advances in Bioreactors for Cell-Based Therapies," *F1000Research*, vol. 7, p. 517, Apr. 2018, doi: 10.12688/f1000research.12533.1. Available: <https://pmc.ncbi.nlm.nih.gov/articles/PMC5931275/>
- 3) Tanja A. Grein, Jasmin Leber, Miriam Blumenstock, Florian Petry, Tobias Weidner, Denise Salzig, Peter Czermak, "Multiphase Mixing Characteristics in a Microcarrier-Based Stirred Tank Bioreactor Suitable for Human Mesenchymal Stem Cell Expansion", *Process Biochemistry*, vol. 51, issue 9, pgs 1109-1119, 2016, ISSN 1359-5113. Available: <https://doi.org/10.1016/j.procbio.2016.05.010>
- 4) D. C. Surrao et al., "Large-Scale Expansion of Human Skin-Derived Precursor Cells (hSKPs) in Stirred Suspension Bioreactors," *Biotechnology and Bioengineering*, vol. 113, no. 12, p. 2725–2738, Jun. 2016, doi: 10.1002/bit.26040. Available: <https://pubmed.ncbi.nlm.nih.gov/27345530/>
- 5) T. Lawson et al., "Process Development for Expansion of Human Mesenchymal Stromal Cells in a 50L Single-Use Stirred Tank Bioreactor," *Biochemical Engineering Journal*, vol. 120, p. 49–62, Nov. 2016, doi: 10.1016/j.bej.2016.11.020. Available: <https://www.sciencedirect.com/science/article/pii/S1369703X16303266>
- 6) S. Markert and K. Joeris, "Establishment of a Fully Automated Microtiter Plate-Based System for Suspension Cell Culture and its Application for Enhanced Process Optimization," *Biotechnology and Bioengineering*, vol. 114, no. 1, p. 113–121, Jul. 2016, doi: 10.1002/bit.26044. Available: <https://pubmed.ncbi.nlm.nih.gov/27399304/>
- 7) M. C. Varley, A. E. Markaki, and R. A. Brooks, "Effect of rotation on scaffold motion and cell growth in rotating bioreactors," *Tissue Engineering Part A*, vol. 23, no. 11–12, p. 522–534, Jan. 2017, doi: 10.1089/ten.tea.2016.0357. Available: <https://pubmed.ncbi.nlm.nih.gov/28125920/>
- 8) B. B. Nguyen, H. Ko, and J. P. Fisher, "Tunable Osteogenic Differentiation of hMPCs in Tubular Perfusion System Bioreactor," *Biotechnology and Bioengineering*, vol. 113, no. 8, p. 1805–1813, Jan. 2016, doi: 10.1002/bit.25929. Available: <https://pubmed.ncbi.nlm.nih.gov/26724678/>
- 9) O. Ball, B.-N. B. Nguyen, J. K. Placone, and J. P. Fisher, "3D printed vascular networks enhance viability in High-Volume perfusion bioreactor," *Annals of Biomedical*

Engineering, vol. 44, no. 12, p. 3435–3445, Jun. 2016, doi: 10.1007/s10439-016-1662-y.
Available: <https://pubmed.ncbi.nlm.nih.gov/27272210/>

- 10) U. Mock et al., “Automated Manufacturing of Chimeric Antigen Receptor T Cells for Adoptive Immunotherapy Using CliniMACS Prodigy,” *Cytotherapy*, vol. 18, no. 8, p. 1002–1011, Jul. 2016, doi: 10.1016/j.jcyt.2016.05.009. Available:
<https://pubmed.ncbi.nlm.nih.gov/27378344/>
- 11) C. Priesner et al., “Automated Enrichment, Transduction, and Expansion of Clinical-Scale CD62L+ T cells for Manufacturing of Gene Therapy Medicinal Products,” *Human Gene Therapy*, vol. 27, no. 10, p. 860–869, Aug. 2016, doi: 10.1089/hum.2016.091.
Available: <https://pubmed.ncbi.nlm.nih.gov/27562135/>